Optical Properties of Two-Dimensional Organic Conductors: Signatures of Charge Ordering and Correlation Effects

Martin Dressel* and Natalia Drichko†

1. Physikalisches Institut, Universität Stuttgart, Pfaffenwaldring 57, D-70550 Stuttgart, Germany

Received February 4, 2004

Contents

1. Introduction 5689
2. Experimental Procedures and Data Analysis 5691
2.1. Experimental Techniques 5691
2.2. Analysis 5692
2.3. Phenomenological Models 5693
2.3.1. Drude-Sommerfeld Model of Free Electrons 5693
2.3.2. Band Anisotropy and Tight-Binding Model 5694
2.3.3. Harmonic Oscillator Describing Phonon Contributions 5694
2.3.4. Interband Transitions 5695
2.4. Intraband and Interband Transitions in the Spectra of Organic Conductors 5695
3. Electron–Phonon Coupling 5696
3.1. Coupling of Electrons with Intramolecular Vibrations 5697
3.2. Assignment of the Observed Vibrational Features 5698
3.3. Probing the Charge on the Molecule 5699
4. Interplay between Structural and Electronic Properties 5699
4.1. Structural Arrangements 5699
4.2. Band Filling versus Electronic-Correlation Effects 5700
4.3. Fingerprints of Electronic Correlations 5701
4.3.1. κ-(BEDT-TTF)$_2X$ 5702
4.3.2. (BEDT-TTF)$_4$[Ni(dto)$_2$] 5702
4.4. Charge Ordering 5703
4.5. Metal-to-Insulator Transition Due to Charge Ordering 5704
4.5.1. α-(BEDT-TTF)$_2$I$_3$ 5705
4.5.2. θ-(BEDT-TTF)$_2MM'$(SCN)$_4$ 5706
4.6. Close to the Charge-Order Transition 5707
4.6.1. α-(BEDT-TTF)$_2M$Hg(SCN)$_4$ 5707
4.6.2. β''-(BEDT-TTF)$_2$SF$_5R$SO$_3$ 5708
4.6.3. β''-(BEDO-TTF)$_5$[MHg(SCN)$_4$]$_2$ 5708
5. Superconductivity 5710
5.1. κ-(BEDT-TTF)$_2$Cu(NCS)$_2$ 5711
5.2. α_t-(BEDT-TTF)$_2$I$_3$ 5711
6. Concluding Remarks 5712
7. Acknowledgments 5713
8. References 5713

* Corresponding author: Phone: +49-711 685 4946. Fax: +49-711 685 4886. E-mail: dressel@pi1.physik.uni-stuttgart.de.
† On leave from Ioffe Physico-Technical Institute, 194021 St. Petersburg, Russia.

1. Introduction

Optical studies, in a broad sense, are one of the most powerful techniques to characterize new materials and to investigate the properties of solids because electromagnetic waves cover a large range of energy and are sensitive to different kinds of excitation. We can obtain information not only on the electronic and the magnetic behavior, but also on the vibrational degrees of freedom, which include lattice properties as well as intramolecular vibrations.[1] In the radio frequency range and below, broad relaxational features can be observed if the lattice becomes soft, as known from ferroelectric phase transitions, but this spectral region is also of superior importance in cases of disorder or some sort of glassy behavior. Collective excitations which are relevant for density waves and other broken-symmetry ground states are located at low frequencies often well below the plasma frequency (Goldstone modes). These ground states of electronic and magnetic long-range order are of particular relevance in low-dimensional metals where the electron gas exhibits the tendency toward instabilities.[2] In the case of superconductivity, the energy gap in the single-particle density of states is expected in an energy range comparable to the superconducting transition temperature, i.e., between microwave frequencies and the far-infrared spectral range. Of particular importance are effects due to electron−electron and electron−phonon interaction, which may lead to a certain frequency dependence of the scattering rate and an enhanced effective mass of the charge carriers.[1] The plasma edge for organic metals is commonly located in the infrared and only for a few exceptions of highly conducting materials even at higher energies. The unequivocal assignment of the optical response to conduction and valence electrons is already difficult in conventional materials if different electronic bands are involved;[1,3−5] in general, no clear-cut distinction is possible in the case of synthetic metals. This fact makes the analysis of optical data of these compounds not a straightforward task, and it is also the reason for many discussions since the early days of molecular conductors. As known from classical semiconductors, interband transitions lead to pronounced signatures in the optical spectrum and can be analyzed in great detail.[6]

10.1021/cr030642f CCC: $48.50
Published on Web 10/27/2004

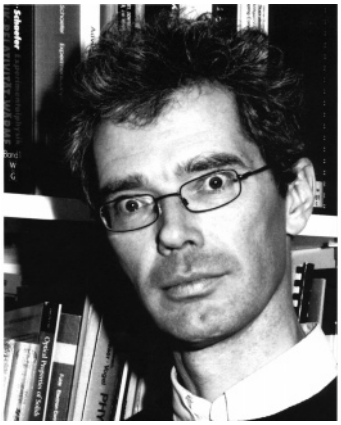

Martin Dressel was born in Bayreuth, Germany, in 1960 and began his study of physics and philosophy at the University Erlangen-Nuremberg. He continued at the Georg-August Universität Göttingen where he received his Diploma and finally his Doctor of Sciences degree in 1989. He continued to work as a postdoctoral research fellow in applied laser science at the Laser-Laboratory Göttingen for two years. Since then he has held positions in the University of British Columbia at Vancouver working with John Eldridge, and at the University of California, Los Angeles, where he stayed for three years in the group of George Grüner as a fellow of the Alexander von Humboldt Foundation. Back in Germany he received his Habilitation at the Technical Universiät Darmstadt in 1996, and then moved to the Center of Electronic Correlations and Magnetism at the Universität Augsburg. Professor Martin Dressel is now Head of the 1. Physikalisches Institut at the Universität Stuttgart. His research covers the electronic and magnetic properties of low-dimensional and correlated electron systems with special focus on organic conductors and superconductors. He is well known for microwave and infrared experiments on TMTSF and BEDT-TTF salts.

Natalia Drichko was born in St. Petersburg, Russia, and received her education in physics at St. Petersburg State University where she graduated in 1996 with a study on the infrared spectra of carbon acids complexes. She continued to work in the field of optical properties of organic materials when she moved to the Ioffe Physico-Technical Institute, St.Petersburg, where she received her Ph.D. degree in 2002 working on fullerenes and conducting organic materials of the BEDT-TTF family and related salts. Frequently, she has been a guest scientist at the Institute of Molecular Physics of the Polish Academy of Sciences at Poznan, Poland; the University of Parma, Italy; and other laboratories. Currently, she pursues her research on the optical properties of quasi-two-dimensional organic conductors as a Alexander von Humboldt fellow at 1. Physikalisches Institut of the Universität Stuttgart. Her areas of expertise are the optical properties of low-dimensional organic solids, in particular, the organic conductors based on the BEDT-TTF molecule and its derivatives. She is interested in the electronic and vibrational properties of these materials.

However, things become more complicated if the symmetry of the lattice is low, if the unit cell is large, and if more than one band contributes to the conductivity.

For the above reasons, the optical behavior has been among the first and most extensively studied properties of organic conductors. A wealth of information is obtained on novel materials, and hence this method is heavily used by a large number of groups all over the world. Frequently, the optical properties of organic conductors have been subject of reviews and extensive discussions.[7−10] Most important in the present context is certainly the series of papers and reviews on TMTSF salts by C. S. Jacobsen in the 1980s.[11−15]

Low-dimensional organic conductors, in general, exhibit a pretty complicated optical response compared to a simple metal such as aluminum or a common semiconductor such as silicon. Hence, most of the models that have been developed during the last century to describe the optical properties of conventional materials are not applicable and need to be adjusted to some extend. Due to the large unit cell with often only one charge carrier mobile, the electronic carrier concentration N is extremely low for synthetic metals compared to aluminum, for instance; for the BEDT-TTF-based compounds the typical values of N are about 10^{21} cm^{-3}. Thus, the Fermi energy E_F is very small in organic metals (around 0.01 to 0.1 eV) and the corresponding temperature T_F becomes comparable to room temperature. The strong anisotropy seems to be an essential element of molecular conductors; it certainly is the source of exciting physical effects. Since many of these phenomena have been observed in organic crystals for the first time, or more clearly than in any other materials, organic compounds became model systems to study physics in reduced dimensions. Starting with Peierls transitions in TTF-TCNQ or TMTTF and TMTSF salts, spin- and charge-density-wave ground states, non-Fermi-liquid and Luttinger-liquid behavior in quasi-one-dimensional metals, recently charge-order and Mott transitions were discovered in one- and two-dimensional organic solids.

In this review, we will give an overview of the infrared optical properties of layered organic conductors: the BEDT-TTF cation-radical salts (where BEDT-TTF or ET stands for bis(ethylenedithio)-tetrathiafulvalene) and their derivatives BEDO-TTF (Figure 1); we will focus on the effects of electronic correlations on the optical properties. On the basis of advanced chemistry and materials science, organic compounds provide the possibility to introduce chemical modifications, which help to vary some electronic or structural parameters more or less independently and thus to deliberately tune the physical properties without affecting the quality of the crystal structure. Modifying the anions or even the organic cations, for instance, changes the overlap integral, the bandwidth, and also the influence of the on-site and intersite Coulomb repulsion. Similarly, the structure of the conducting layer can be altered since most compounds crystallize in a large number of different

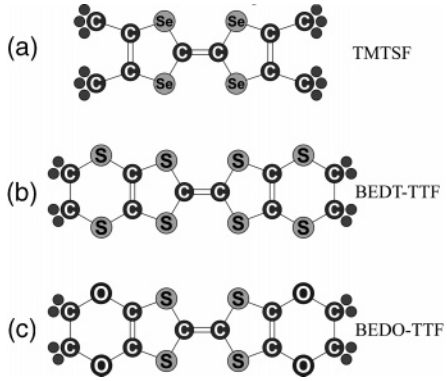

Figure 1. Organic molecules: (a) TMTSF, (b) BEDT-TTF, (c) BEDO-TTF. The molecules are basically flat, with only the ethylene groups slightly tilted out of the plane.

phases, often with distinct physical properties. A different stoichiometry, crystallographic phase, or change of anions can vary the band filling, which might turn an insulator to a metal, for instance.

2. Experimental Procedures and Data Analysis

2.1. Experimental Techniques

Investigations of the optical properties of conducting solids are normally performed by reflection measurements covering the spectral range from the far-infrared up to the ultraviolet. In the frequency region from 10^4 to 10^6 cm^{-1} (visible and ultraviolet), grating spectrometers are utilized. In this spectral range, normally the intramolecular electronic transitions of BEDT-TTF and sometimes of the molecules from the anion layer are observed. The infrared region (10 to 10^4 cm^{-1}) is covered by Fourier transform spectrometers; a typical setup is sketched in Figure 2. For investigations of small-sized samples, microscopes are employed; they make it possible to measure the optical reflectivity on a spot size of less than 0.1 mm. The infrared microscopes operate in a frequency range of 200−10 000 cm^{-1};[16] thus, it is possible to observe the plasma edge, interband transitions, and intramolecular vibrations. The optical features that appear due to correlation effects and collective excitations lie at lower frequencies; to study them it is necessary to perform measurements in the frequency range down to about 10 cm^{-1}. Special coherent source submillimeter spectrometers are successfully utilized in this range.[17] The use of suitable polarizers makes it possible to probe the anisotropy of the sample plane whenever required.

To obtain absolute values of the reflectivity, the sample is in general replaced by a gold or aluminum mirror (evaporated metal film on a glass substrate), which is commonly done either by rotation or translation. In any case, the reference has to be put exactly in the same position as the sample; this becomes increasingly important for highly conducting samples at low frequencies where the reflectivity is close to unity.[18] With respect to reproducibility, diffraction effects, standing wave pattern at low frequencies, it is advantageous to use a single aperture and exchange sample and reference behind this aperture. A sketch of our setup which is employed to study reflectance in a wide range of frequency (10−7000 cm^{-1}) is displayed in Figure 3.

In particular in the far-infrared range, diffraction becomes a serious problem for the investigation of single crystals because the sample size should reach at least three to five times the wavelength, meaning that for a typical sample of 1 mm diameter one should proceed with caution below 50 cm^{-1}. Sometimes mosaics are assembled, but it is not always possible to overcome the difficulties of surface roughness and gaps between the crystallites. In certain cases, the sample can be covered by gold or silver (thickness about 300 nm) and remeasured for reference;[19] the influence of diffraction effects should

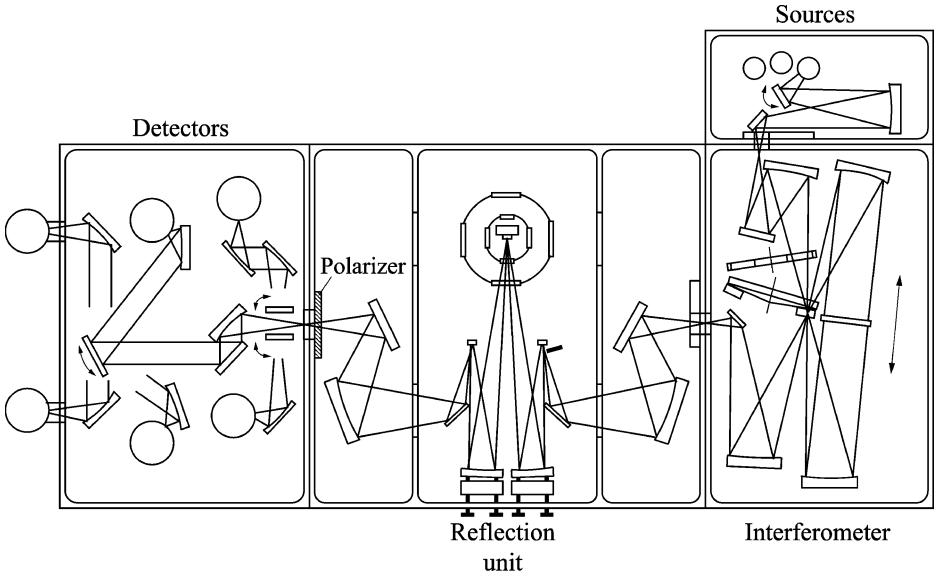

Figure 2. Optical layout of a modified Bruker IFS 113v Fourier transform interferometer. The infrared radiation is selected from three different sources, guided through aperture and filter to the Michelson interferometer with six beamsplitter to choose from. A switching chamber enables one to perform either transmission or reflection measurements of the sample inside the cryostat. The light is detected by one of six detectors; two of them are helium-cooled Si bolometers, and two are cooled by liquid nitrogen.

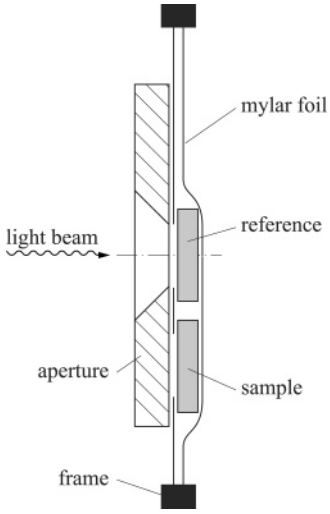

Figure 3. Sectional drawing of a sample holder used for optical reflection measurements in the infrared spectral range. The sample and reference are placed between two thin Mylar foils spanned in a metal frame, which can be moved. A hole slightly smaller than the sample is cut into the sheet through which the optical reflection measurements are performed.

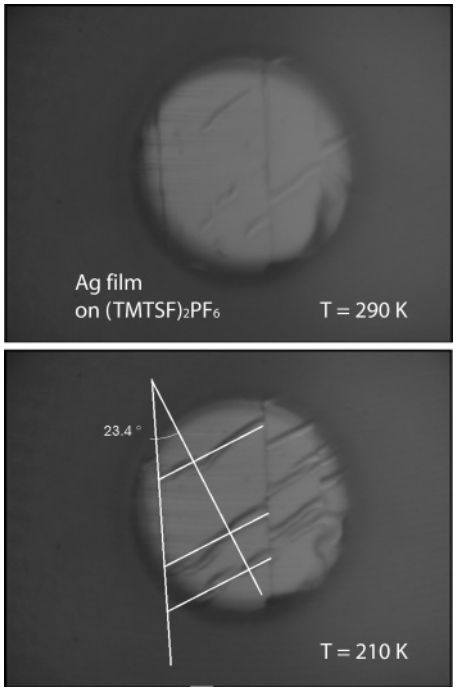

Figure 4. Silver film deposited on a $(TMTSF)_2PF_6$ crystal with the a-axis pointing up; the spot size has a diameter of 200 μm. The upper frame shows the film at room temperature; the photograph in the lower frame is taken at T = 210 K. Because the thermal contraction of the organic crystals is much larger compared to the metal, the film becomes wrinkled upon cooling, but stretches again in a reproducible way when warmed. The ratio of the thermal expansion parallel (1.4%) and perpendicular (0.4%)[21] to the stacking direction (a and b'-axes) corresponds to the 23.4 ° angle observed between wrinkles and stacks.[20]

cancel. However, the large thermal contraction of organic solids causes serious distortions in the metal films upon cooling, as demonstrated in Figure 4. Recently, a near-field spectrometer was developed operating in the far-infrared range and below;[20] it permits one to probe the absorption of a crystal on a spot size of 100 μm or less.

Because in most cases the temperature dependence of the optical reflectivity is of interest, the crystals are placed in an optical cryostat by which temperatures as low as 4 K are achieved, in some cases even lower. To perform optical experiments in the presence of a magnetic field, magnetocryostats with optical windows are employed. In a superconducting split-coil arrangement measurements parallel and perpendicular to the magnetic field $B \leq 12$ T can be conducted.

2.2. Analysis

By measuring the optical reflectivity $R(\omega)$ over a wide spectral range, we can obtain the complex electrodynamic response. The Kramers−Kronig relations give the phase shift $\phi_r(\omega)$ of the reflected signal as

$$\phi_r(\omega) = \frac{\omega}{\pi}\int_0^\infty \frac{\ln\{R(\omega')\} - \ln\{R(\omega)\}}{\omega^2 - \omega'^2}\,d\omega' \qquad (1)$$

which then permits the calculation of the complex conductivity $\hat{\sigma} = \sigma_1 + i\sigma_2$ and dielectric constant $\hat{\epsilon} = \epsilon_1 + i\epsilon_2$:

$$\sigma_1(\omega) = \frac{\omega}{4\pi}\epsilon_2(\omega) = \frac{\omega}{4\pi}\frac{4\sqrt{R(\omega)}[1 - R(\omega)]\sin\phi_r}{[1 + R(\omega) - 2\sqrt{R(\omega)}\cos\phi_r]^2} \qquad (2)$$

$$\sigma_2(\omega) = \frac{\omega}{4\pi}[1 - \epsilon_1(\omega)] = \frac{\omega}{4\pi}\left(1 - \frac{[1 - R(\omega)]^2 - 4R(\omega)\sin^2\phi_r}{[1 + R(\omega) - 2\sqrt{R(\omega)}\cos\phi_r]^2}\right) \qquad (3)$$

at the normal incidence of light, using the well-known relations between the conductivity and the reflectivity.[1] The refractive index n, the extinction coefficient k, and the absorption coefficient $\alpha = 2k\omega/c$ are related to the dielectric constant ϵ_1 and the conductivity σ_1, which denote the change of the fields and current upon the presence of matter:

$$n + ik = \left[\epsilon_1 + i\frac{4\pi\sigma_1}{\omega}\right]^{1/2} = \hat{\epsilon}^{1/2} \qquad (4)$$

assuming that the material has negligible magnetic properties: $\mu_1 = 1$.

The extrapolation beyond the low- and high-frequency end of the experimental data is of great significance to perform the Kramers−Kronig analysis. At high frequencies, the reflectivity $R(\omega)$ will eventually approach zero and most commonly a $R(\omega) \propto \omega^{-2}$ behavior is assumed; sometimes an even faster drop with ω^{-4} is used well above the visible range. More problematic is the low-frequency extrapolation. For an insulating (or semiconducting) material, the reflectivity is assumed to remain constant for $\omega \rightarrow 0$. However, this will inevitably lead to a vanishing conductivity for zero frequency; often in contrast to the measured properties of poor, but not zero conductivity. To obtain a finite dc conductivity,

the extrapolation of $R(\omega)$ has to lead to unity for $\omega \rightarrow 0$; there are different approaches to do so. On the basis of the Drude model, the Hagen-Rubens law

$$R(\omega) \approx 1 - \left(\frac{2\omega}{\pi\sigma_{dc}}\right)^{1/2} \quad (5)$$

describes the reflectivity of metals below the scattering rate $\omega < 1/\tau$. It can be used to connect the lowest experimental point of the reflectivity data with $R = 1$ at $\omega = 0$, leading to a certain value for $\sigma_1(\omega \rightarrow 0)$, which may be called the optical dc value. If dc measurements were performed or reliable data are available, σ_{dc} can be used to calculate $R(\omega)$ within the Hagen-Rubens approximation. However, discrepancies between $\sigma_1(\omega \rightarrow 0)$ and the measured dc conductivity are common for low-dimensional conductors and other unconventional metals. The reason can be found in low-energy excitations, in some power-law conductivity due to the reduced dimensionality, or due to nonmetallic transport mechanisms, such as hopping or relaxational processes.[1] It is worthwhile to have a closer look into the low-frequency behavior of correlated electron systems, where numerous interesting physical effects can be studied; only some of them will be mentioned in the following section.

2.3. Phenomenological Models

The optical response of solids may contain contributions from conduction electrons, interband transitions, and phonons; a typical behavior is plotted in Figure 5. In the present case due to the large organic molecules, intramolecular phonons are of equal importance as intermolecular lattice vibrations. To separate those contributions and to analyze them, phenomenological models are widely applied for a first approximation and to draw first conclusions.

2.3.1. Drude-Sommerfeld Model of Free Electrons

In the classical approach of noninteracting electrons, P. Drude developed a simple but powerful model to describe the optical properties of metals. The main assumption of this approach is that the density of states is approximately constant in the relevant energy range, and the low-frequency conductivity is solely determined by the scattering rate.[1] The charged particles of density N and mass m are accelerated by the alternating electric field $E(t) = E_0\exp\{-i\omega t\}$. After travelling a certain distance, the so-called mean free path l, they experience collisions and lose their momentum. The frequency dependent conductivity is then given by

$$\hat{\sigma}(\omega) = \frac{Ne^2\tau}{m}\frac{1}{1 - i\omega\tau} = \frac{Ne^2\tau}{m}\frac{1 - i\omega\tau}{1 + \omega^2\tau^2} \quad (6)$$

Here τ is the relaxation or scattering time between two collisions, which is related to the mean free path

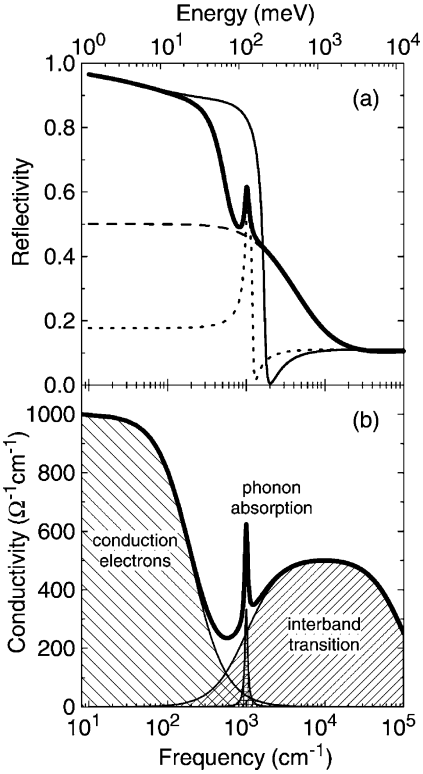

Figure 5. Model of the frequency dependent (a) reflectivity and (b) conductivity of a typical organic metal containing three contributions. (i) The metallic behavior of the conduction electrons is described by the Drude model (eq 6) for the plasma frequency $\omega_p/(2\pi c) = 1000$ cm^{-1} an the scattering rate $1/(2\pi c\tau) = 200$ cm^{-1} (thin solid line). (ii) The interband transitions between 10^3 and 10^5 cm^{-1} are modeled by an overdamped oscillator (dashed line). (iii) A phonon at 1000 cm^{-1} is described by the Lorentz model (eq 20) (dotted line). The total conductivity $\sigma_1(\omega)$ and reflectivity $R(\omega)$ are shown by the thick solid line.

by the Fermi velocity: $l = v_F\tau$ as introduced by A. Sommerfeld. The sum rule

$$\int_0^\infty \sigma_1(\omega)\, d\omega = \frac{\pi Ne^2}{2m} = \frac{\omega_p^2}{8} \quad (7)$$

connects the area under the conductivity curve to the plasma frequency

$$\omega_p = \left(\frac{4\pi Ne^2}{m}\right)^{1/2} \quad (8)$$

Commonly effects of electron−phonon interaction and electron−electron interaction are treated by a renormalized mass, called the bandmass or effective mass (see subsequent section). Assuming the carrier mass m, the plasma frequency measures the number of free carriers N; vice versa, ω_p allows us to evaluate the effective mass and thus correlation effects if we know the density of charge carriers. The dc limit of the conductivity is

$$\sigma_1(\omega = 0) = \sigma_{dc} = \frac{Ne^2\tau}{m} \quad (9)$$

In the low-frequency or Hagen-Rubens regime, defined by the condition $\omega\tau \ll 1$, the optical properties are fully determined by the dc conductivity σ_{dc}; for

the real part of the conductivity σ_1 is frequency independent: $\sigma_{dc} \approx \sigma_1(\omega)$.

2.3.2. Band Anisotropy and Tight-Binding Model

For real materials, the interaction with the underlying lattice together with electron−electron and electron−phonon interactions call for corrections to the above description. Broadly speaking, these effects can be summarized assuming an effective mass, which is different from the free-electron mass and may, in general, be frequency dependent. The simplest case of quasi-free electrons considers the scattering of the electrons on the periodic potential and leads to the introduction of the bandmass m_b given by the curvature of the energy band $\epsilon(\boldsymbol{k})$ in $\boldsymbol{k}$ space

$$\frac{1}{m_b} = \frac{1}{\hbar^2}\frac{\partial^2\epsilon(\boldsymbol{k})}{\partial \boldsymbol{k}^2} \tag{10}$$

The bandmass m_b may be anisotropic and then the plasma frequency $\omega_p = \sqrt{4\pi Ne^2/m_b}$, for instance, depends on the orientation of the electric field with respect to the crystallographic axes.

Band structure effects can be described by the Boltzmann equation where the electron velocity is related to the applied electric field of direction $\boldsymbol{n}_E$. For $T = 0$ we obtain[1]

$$\hat{\sigma}(\omega) = \frac{2e^2}{(2\pi)^3\hbar}\int_{\epsilon=\epsilon_F}\frac{(\boldsymbol{n}_E\cdot\boldsymbol{v}_k)\tau}{1 - i\omega\tau}\,dS_F \tag{11}$$

where is integration is carried out over the Fermi surface S_F. As $\sigma_1 = Ne^2\tau/m$, one can define an effective mass $1/m \propto \int \boldsymbol{n}_E\cdot\boldsymbol{v}_k\,dS_F$ which, in general, will also depend on the orientation of the applied electric field $\boldsymbol{E}$. Here ϵ_F is the Fermi energy, $\boldsymbol{v}_k$ is the velocity of the charge carriers for a given wavevector $\boldsymbol{k}$.

Such effects are particularly important when the band structure is highly anisotropic. The simplest model for the one-dimensional organic conductors assumes non-interacting electrons that move along a chain.[11,14,15] The tight-binding approximation leads to a cosine energy band:

$$\epsilon(k) = \epsilon_0 + 2t\cos\{kd\} \tag{12}$$

with t the transfer integral associated with the finite overlap between neighboring orbitals, and d the molecular distance; the bandwidth is $W = 4t$. In the following, we are mainly interested in the highest occupied molecular orbitals (HOMO) that form the conduction band; they are located around the energy level ϵ_0. With ρ electrons per site, the band is filled up to $\pm k_F = \pm\pi\rho/2d$. For this simple one-dimensional model, the Fermi surface consists of two parallel sheets at $k = \pm k_F$ and the density of states is given by

$$D(\epsilon_F) = \left(\pi\sin\left\{\frac{\pi}{2}\rho\right\}\right)^{-1} \tag{13}$$

The plasma frequency can be calculated from

$$\omega_p{}^2 = \frac{4\pi e^2}{\hbar^2}\sum_{BZ} f(\epsilon_k)\frac{\partial^2\epsilon_k}{\partial k^2} \tag{14}$$

$$= \frac{16td^2e^2}{\hbar^2 V_m}\sin\left\{\frac{\pi}{2}\rho\right\} \tag{15}$$

where V_m is the volume per molecule, i.e., the unit-cell volume divided by the number of organic molecules per unit cell.

In the case of two-dimensional conductors, the interaction between the chains has to be considered and the hopping integrals $t_{||}$ and $t_\perp$ are defined:

$$\epsilon(k) = \epsilon_0 + 2t_{||}\cos\{k_{||}d_{||}\} + 2t_\perp\cos\{k_\perp d_\perp\} \tag{16}$$

For appreciable $t_\perp \approx t_{||}$ the Fermi surface will be closed, i.e., cylindrical. In the limit of $t_\perp \ll t_{||}$ only a warping of the Fermi surface is introduced by the small $t_\perp$ as a perturbation of the one-dimensional sheets. Then the plasma frequency is given by

$$\omega_{p\perp}{}^2 = \frac{2}{\pi\sin\{\rho\pi/2\}}\frac{4\pi e^2 d_\perp{}^2}{\hbar^2 V_m}\frac{t_\perp{}^2}{t_{||}} \tag{17}$$

which is reduced by the bandwidth anisotropy

$$\left(\frac{\omega_{p\perp}}{\omega_{p||}}\right)^2 \propto \left(\frac{t_\perp}{t_{||}}\right)^2 \tag{18}$$

Rather early, it was found that the ratio of the transfer integrals is consistent with the anisotropy ratio experimentally obtained from the dc conductivity[22−24]

$$\frac{\sigma_{||}}{\sigma_\perp} \propto \left(\frac{t_{||}}{t_\perp}\right)^2 \tag{19}$$

2.3.3. Harmonic Oscillator Describing Phonon Contributions

In a first approach, the absorption of electromagnetic waves by phonons is approximated by the Lorentz model. For the complex dielectric constant, we can write[1]

$$\hat{\epsilon}(\omega) = 1 + \frac{\omega_p{}^2}{(\omega_0{}^2 - \omega^2) - i\omega/\tau} \tag{20}$$

ω_0 is the center frequency, often called the oscillator frequency, $1/\tau$ denotes the broadening of the oscillator due to damping, $\omega_p = (4\pi Ne^2/m)^{1/2}$ describes the oscillator strength, and is also referred to as the plasma frequency. The above eq 20 can be expressed in terms of the optical conductivity and split into real and imaginary parts:

$$\sigma_1(\omega) = \frac{{\omega_p}^2}{4\pi} \frac{\omega^2/\tau}{({\omega_0}^2 - \omega^2)^2 + \omega^2/\tau^2} \text{ and}$$

$$\sigma_2(\omega) = -\frac{{\omega_p}^2}{4\pi} \frac{\omega({\omega_0}^2 - \omega^2)}{({\omega_0}^2 - \omega^2)^2 + \omega^2/\tau^2} \quad (21)$$

A more advanced discussion of the vibrational properties is given below in Section 3.

2.3.4. Interband Transitions

Compared to the modeling of free electrons and phonon features, the description of interband transitions is not straightforward. The main difficulty faced is that the density of the electronic states of valence and conduction band explicitly enters the optical conductivity:[1,6]

$$\sigma_1(\omega) = \frac{\pi e^2}{m^2 \omega} \sum_{l,l'} D_{l'l}(\hbar\omega) |\boldsymbol{p}_{l'l}|^2 \quad (22)$$

where

$$D_{l'l}(\hbar\omega) = \frac{2}{(2\pi)^3} \int_{\hbar\omega = \epsilon_{l'l}} \frac{dS_\epsilon}{|\nabla_{\boldsymbol{k}}[\epsilon_{l'}(\boldsymbol{k}) - \epsilon_l(\boldsymbol{k})]|} \quad (23)$$

is the joint density of states between the band l and l' described by the energy dispersion $\epsilon_l(\boldsymbol{k})$ and $\epsilon_{l'}(\boldsymbol{k})$, and $\boldsymbol{p}_{l'l}$ is the electric dipole matrix element which determines the probability of transitions depending on the wave functions involved. Hence, the calculation of the joint density of states requires knowledge of the actual band structure, which in general cannot be solved adequately; even less is known about the matrix element. Near to the band edge, parabolic bands are commonly assumed in three dimensions; an assumption that is certainly not correct in two and one dimensions, where instead step functions or singularities are expected. This behavior is rarely observed for anisotropic band semiconductors (for example, in KCP or $(NbSe_4)_3I$[25,26]), but important in the case of narrow energy gaps, which open due to electronic correlations such as density waves or Mott−Hubbard transitions.[1,2]

The contributions of the interband transitions to the optical conductivity usually show up as broad bands in the mid- and near-infrared region, but also all the way up to the visible and above. Commonly, they are modeled by a number of Lorentz oscillators[1]

$$\hat{\sigma}(\omega) = \sum_j \frac{{\omega_{pj}}^2}{4\pi} \frac{\omega}{i({\omega_{0j}}^2 - \omega^2) + \omega/\tau_j} \quad (24)$$

Only if j is kept to a minimum and the relative dependence on temperature, doping, or other variation of the material is monitored, this phenomenological approach leads to some insight. Examples are the exchange of intensity between interband transitions, the shift of frequency, etc. due to phase transitions or ordering phenomena (see Section 4.4 below).

The energy gap between valence and conduction bands is often masked by an additional free-electron contribution, by multiband contributions, indirect transitions, or phonon effects, in particular, at high temperatures. One possible estimate for the semiconducting gap is the linear extrapolation of the leading edge of the band to the abscissa; sometimes a square root behavior is more appropriate. The subtraction of the contributions of quasi-free electrons [fitted by the Drude model eq 6] and from phonons [fitted by harmonic oscillators eq 20] should reveal to the interband excitations that contribute to the optical conductivity without assuming a particular shape (cf. Figure 5).

2.4. Intraband and Interband Transitions in the Spectra of Organic Conductors

In first approximation, these simple phenomenological models describe the optical properties of organic conductors quite well. The standard procedure is to fit the measured reflectivity and conductivity spectra by a Drude formula (6)—thus describing only intraband excitations—or a sum of Drude and Lorentz contributions [eqs 6 and 24]—describing both intra- and interband transitions as depicted in Figure 5. In many cases, however, a clear-cut distinction between intra- and interband contributions is not possible. The determination of the plasma frequency ω_p by integrating the optical conductivity

$${\omega^2}_p = 8 \int_0^{\omega_c} \sigma_1(\omega)\, d\omega \quad (25)$$

very much depends on the choice of the upper cutoff frequency ω_c, and there is no simple and general solution.

It was pointed out by many authors that commonly in the room temperature spectra of organic conductors the Drude term is very weak, if present at all. For the example of the two-dimensional metal β-(BEDT-TTF)$_2$I$_3$, H. Tajima et al.[27] used band-structure calculations to estimate a Drude oscillator strength at $T = 300$ K. They found the value to be about 6 to 7 times lower than that for the interband transitions. The overall oscillator strength calculated by eq 7, however, is in agreement with the value estimated from the dc conductivity by eqs 8 and 9. The optical reflectivity $R(\omega)$ and conductivity $\sigma_1(\omega)$ for both polarizations parallel and perpendicular to the stacks are plotted in Figure 6. An estimate of the transfer integrals for β-(BEDT-TTF)$_2$I$_3$ using the optical data measured at $T = 40$ K was performed by C. S. Jacobsen et al.[28] The plasma frequencies are obtained by a Drude fit of the reflectivity spectra measured in two polarization directions with the largest anisotropy in the conducting plane. Using eqs 15 and 17 the transfer integrals were calculated: $t_{\parallel} \approx 0.10$ eV, and $t_{\perp} \approx 0.13$ eV. This gives a very small anisotropy ($t_{\parallel}/t_{\perp} \approx 0.75$) within the conducting plane, and therefore the Fermi surface is expected to be of a cylindrical shape. These results agree with measurements of the nearly isotropic dc conductivity in the conducting plane [eq 19] and with band-structure calculations.

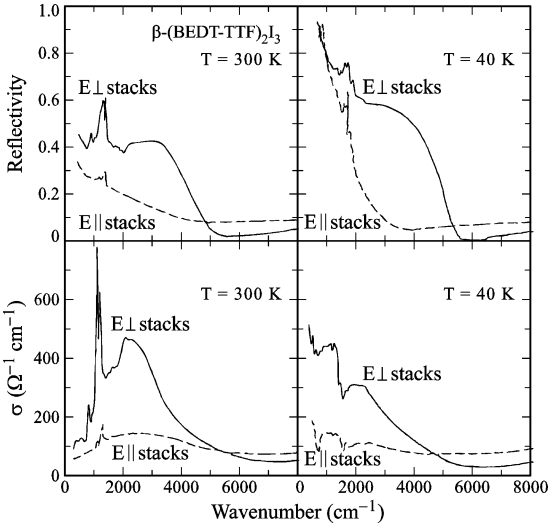

Figure 6. Polarized reflectivity spectra of β-(BEDT-TTF)$_2$I$_3$ measured for the electric field E polarized parallel and E perpendicular to the stacks of BEDT-TTF molecules at room temperature (left panels) and 40 K (right panels). No clear Drude component is observed at room temperature, although the dc conductivity is fairly good. The plasma frequency was estimated by a fit using the Drude formula in the range around plasma edge and reflectivity minimum (adapted with permission from ref 28).

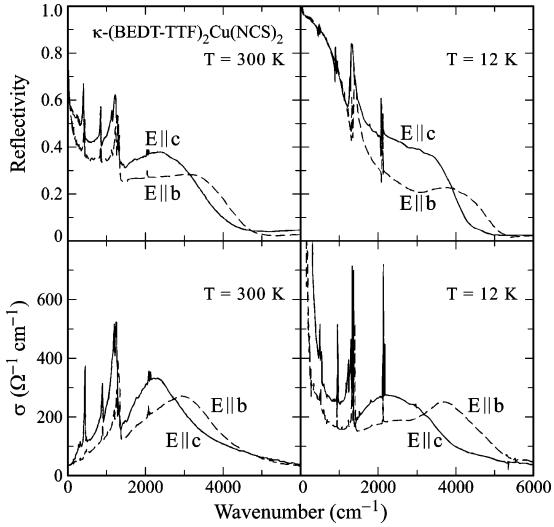

Figure 7. Frequency dependence of the reflectivity and conductivity of κ-(BEDT-TTF)$_2$Cu(NCS)$_2$ at T = 300 and 12 K for E || b and E || c, respectively. The narrow Drude contribution appears only below 50 K (adapted with permission from ref 31).

In the spectra of most of the quasi-two-dimensional organic conductors a mid-infrared band with a maximum at 2000 to 3000 cm^{-1} is observed; it normally can be fitted by a Lorentz oscillator. The dependence of its intensity on the structure of the conducting layer led to an assignment of this band to the interband transitions, where the gap between the bands appears due to dimerizations of the molecules in the structure.[29] On the other hand, H. Tajima et al.[30] assigned this wide mid-infrared band in the spectra of non-dimerized θ-phase to an interband transition between bands split by charge ordering.

This band is especially intensive in the spectra of the κ-phase compounds, for example, κ-(BEDT-TTF)$_2$[Cu(SCN)$_2$] and κ-(BEDT-TTF)$_2$[N(CN)$_2$Br] (Figure 7); based on the calculated band structure it was assigned to interband transitions.[32,33] Alternatively, N. L. Wang et al.[34] suggested that the broad peak observed in the room temperature optical conductivity of κ-(BEDT-TTF)$_2$Cu(NCS)$_2$ at 2300 and 3700 cm^{-1} in the c and b direction, respectively, can be explained by photon-assisted hopping of small polarons which are basically localized at high temperatures. At low temperatures, large polarons dominate the optical response in the form of coherent (Drude-like peak) and incoherent (mid-infrared band) transport.

As already mentioned, a Drude component is absent in the room temperature spectra of the κ-phase, and only a narrow zero-frequency contribution appears in the spectra at temperatures below 50 K. This behavior cannot be explained in the framework of the simple Drude-Lorentz picture, but by advanced models of R. McKenzie and J. Merino,[35−38] which take into account electronic correlations (see Section 4.3.1). Similarly for the superconductor β''-(BEDT-TTF)$_2$SF$_5$CH$_2$CF$_2$SO$_3$, the absence of a Drude peak in the spectra down to T = 10 K is reported by J. Dong et al.[39] (cf. Section 4.6.2), pointing in the direction of a more general behavior of organic superconductors.

3. Electron−Phonon Coupling

One of the striking features commonly observed in the infrared spectra of organic conductors are the narrow bands at frequencies of BEDT-TTF intramolecular vibrations, which are superimposed on the electronic background (e.g., Figure 7). They have asymmetric shapes, characteristic for a single level interacting with a continuum of states (Fano effect).[40] These features are caused by electronic excitations which couple to intramolecular vibrations, the so-called electron-molecular vibration (EMV) coupling.

Compared to conventional metals and semiconductors, the building blocks of synthetic metals are large molecules, a fact that has appreciable effects on the vibrational and electronic properties. In general, we can distinguish two sorts of electron−phonon interaction: a coupling to lattice phonons that is normally found in any kinds of solid, and a coupling of the electrons to intramolecular vibrations of the BEDT-TTF molecule (or other organic molecules that form the conducting layer). Within the framework of the tight-binding description of electrons (cf. Section 2.3.2), the difference between these two effects is that the coupling to lattice vibrations modulates the transfer integrals t, while the coupling to intramolecular vibrations modulates the on-site energy ϵ.[41] The energy of these two kinds of phonons is also distinct: due to the comparably heavy molecules the lattice modes are observed below approximately 200 cm^{-1} for these crystals, while the intramolecular vibrations of BEDT-TTF, which show the strongest coupling constants, lie between 400 and 1600 cm^{-1}.

The electron−phonon coupling is one of the mechanisms frequently suggested to be relevant for superconductivity in organic conductors,[24,42] and the high frequencies of the intramolecular vibrations

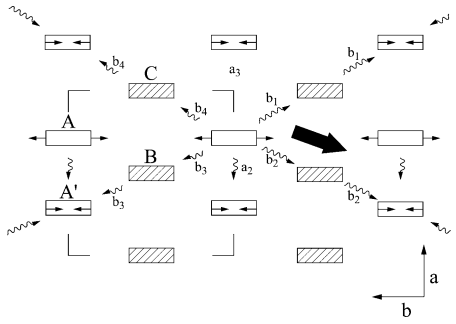

Figure 8. Sketch of the charge flow in the out-of-phase vibrating A and A′ molecules. The small arrows indicate the charge flow induced by the vibrations, and the big arrow represents the resulting charge flow. a_2, a_3, b_1, b_2, b_3, and b_4 indicate the transfer integrals introduced by T. Mori et al.[51] (Reprinted with permission from ref 44. Copyright 1986 Les Éditions de Physique.)

were proposed to cause the comparably high transition temperature T_c. These considerations — but also the fact that intramolecular vibrations are very sensitive to changes of the charge on the BEDT-TTF molecules and to their symmetry — make molecular vibrations a very interesting and important topic.

3.1. Coupling of Electrons with Intramolecular Vibrations

The coupling of electrons to molecular vibrations was first observed and described for one-dimensional systems (see for example review ref 43). This model still is the basis to explain the EMV-coupling also in two-dimensional organic conductors. The interaction takes place via a modulation of the HOMO energy;[44] for one dimension in the presence of a symmetry break the EMV interaction induces oscillations of the conduction electron density along the stacking direction with the frequency of the phonons;[45−49] hence, the excitations couple to the external infrared radiation. In this context, symmetry break means that the molecular units should not lie at the inversion centers. It was shown for one-dimensional systems that if the occupied molecular orbital is nondegenerate, the linear EMV-coupling is possible only to the totally symmetric A_g vibrational modes of the molecule,[50] which normally are infrared forbidden.

In ref 44, a qualitative picture of the EMV-coupling for the two-dimensional case was proposed and specified on the example of α-(BEDT-TTF)$_2$I$_3$. In the α-phase two molecules in stack 1 (A and A′) are connected by an inversion center, and the other two molecules in the unit cell (B and C in stack 2) lie on the centers of inversion as displayed in Figure 8. The D_2 symmetry of the BEDT-TTF molecule is lowered in the crystal lattice according to the scheme given in Figure 9. The symmetry of the vibrations changes respectively: the totally symmetric (A symmetry) vibrations of the A + A′ dimer give rise to both A_g (infrared forbidden but Raman active) and A_u (infrared active) vibrations, while the molecules B and C, which lie on the inversion centers, give rise only to infrared forbidden A_g vibrations (Figure 9). The A_u vibration of the A + A′ dimer implies an out-of-phase motion of these molecules, which modulates the on-site energy ϵ; this modulation induces a charge flow.

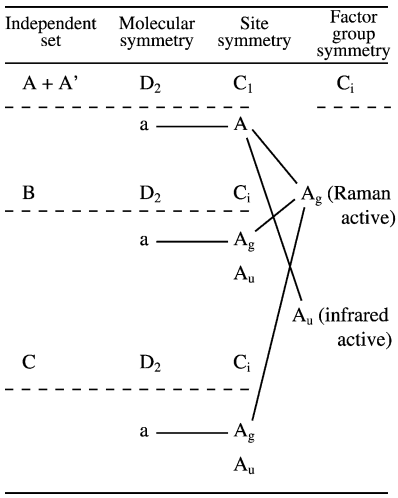

Figure 9. Symmetry correlations for BEDT-TTF totally symmetric modes in the example of α-(BEDT-TTF)$_2$I$_3$. (Reprinted with permission from ref 44. Copyright 1986 Les Éditions de Physique.)

The dipole moment results from the differences between the transfer integrals on the opposite sides of the molecule. A scheme of this process is reproduced in Figure 8. The charge flow couples to the infrared radiation: in the optical spectra we can observe the vibrational features activated by the charge flow (i.e., EMV-coupled features) at the frequencies of these A_g vibrations of the BEDT-TTF molecule. The scheme shows that the molecules which participate in EMV-coupling do not lie on the inversion centers, and EMV-coupling gets stronger with increasing lattice distortion (i.e., the displacement of the molecules from the possible inversion centers).

The strength of the EMV-coupling is characterized by the coupling constants g_j (where the subscript j indicates the normal coordinate of the molecule), which are defined as the energy variation of the HOMO level ϵ on the change of the respective normal coordinate of the molecule Q_j:

$$g_j = \frac{\partial E}{\partial Q_j} \tag{26}$$

These constants can be obtained by a comparison of experimental optical conductivity spectra to theoretical calculations which take into account the EMV-coupling. Results of this treatment for a number of BEDT-TTF salts are summarized in ref 52. Another experimental method to determine g_j is based on a comparison of optical conductivity and Raman data (see ref 53). The values of g_j experimentally determined by optical experiments are 43 and 71 meV for the ν_2 and ν_3 modes, respectively. Similar results are obtained by the first method.

As was shown above, the broken symmetry is essential for EMV-coupling. Indeed, the strength of the EMV-coupled features significantly depends on the arrangement of the BEDT-TTF molecules in the conducting layer, being more prominent in dimerized structures; consequently, this effect is strongest in the κ-phase. Therefore, the strength of the EMV-coupling provides a distinction of different phases

(see Section 3.3) and to characterize them with respect to their dimerization. In fact, the observation of the EMV-coupled features in infrared spectra makes it possible to follow phase transitions associated with structural changes and charge ordering (cf. Section 4.4 below).

The cluster approach of V. M. Yartsev[54−56] to calculate the optical properties is unique because it describes both the electronic part and the EMV-coupling. The optical properties are first calculated for a certain isolated ($U \rightarrow \infty$) cluster of BEDT-TTF molecules, and in a next step the resulting spectrum is constructed by a superposition of the spectra of these clusters. This model was successfully applied to describe the κ-phase spectrum. For the orthogonal dimers, a charge transfer within the dimers and between the dimers is taken into account. A charge-transfer band shows up in the spectra as a wide maximum in the mid-infrared region, and its position depends on the microscopic parameters: on the transfer integrals between the molecules and on-site Coulomb repulsion U. The larger the value of the on-site repulsion, the more the shape of the spectrum is similar to the one of the isolated dimer. The charge transfer between the molecules activates the intramolecular A_g vibrations of BEDT-TTF. The frequencies of the vibrational features are related to the position of its maximum: when the electronic maximum shifts to higher frequencies, the coupled features also move up in frequency (the coupling becomes weaker). A fit of the experimental spectra of the κ-phase compounds by this model yields the EMV-coupling constants.[55,56]

3.2. Assignment of the Observed Vibrational Features

Most of the vibrational features, which are observed in the infrared spectra, can be assigned to intramolecular vibrations of BEDT-TTF activated by EMV-coupling on the basis of a normal-coordinate analysis. The BEDT-TTF vibrations have been calculated applying different methods; a detailed comparison of their results can be found in ref 52. Because the BEDT-TTF molecule is slightly bent in a crystal, it has a D_2 symmetry leading to 19 A_g modes;[44] hence, all the typically observed EMV-coupled features can be assigned to A_g vibrations.

In a flat-molecule approximation, the symmetry of BEDT-TTF increases to D_{2h}, which results in 12 A_g modes (Figure 10) calculated by M. E. Kozlov et al.[57,58] for a neutral BEDT-TTF molecule and ionized BEDT-TTF$^+$. Their assignment is based on infrared absorbance and Raman spectra of the BEDT-TTF and d_8-BEDT-TTF molecules and their cation-radical salts. The assumption of a planar molecule simplifies the calculations appreciably but still yields good agreement with the experiment, although not all of the observed EMV-coupled features can be assigned to A_g vibrations.[59−61]

The calculation of the normal-mode vibrations of the BEDT-TTF molecule—still assuming D_{2h} symmetry—and the assignment of experimentally observed infrared and Raman spectra of natural and isotope-substituted BEDT-TTF molecules was improved by J. Eldridge et al.;[62] the results are displayed in Figure 10. Among the A_g modes only the C−H vibrations $\nu_7(A_g)$ differ from the previous approach.[57] He argued[59,60] that in two dimensions an EMV-coupling to B_{3g} vibrations is also possible, for example, to the $\nu_{60}(B_{3g})$ mode, which involves the out-of-phase vibrations of the two C=C bonds at the rings of the BEDT-TTF molecule. If the molecules in a dimer (such as in the κ-phase) vibrate out of phase, the overlap of their orbitals changes; this leads to a charge transfer between adjacent dimers. However, J. Eldridge[63] now agrees with the results of recent calculations by A. Girlando et al.[64] that the strong feature at 890 cm^{-1} in both the Raman and infrared spectra should be assigned to $\nu_{10}(A_g)$, assuming only D_2 point group symmetry for the BEDT-TTF$^+$ molecule.

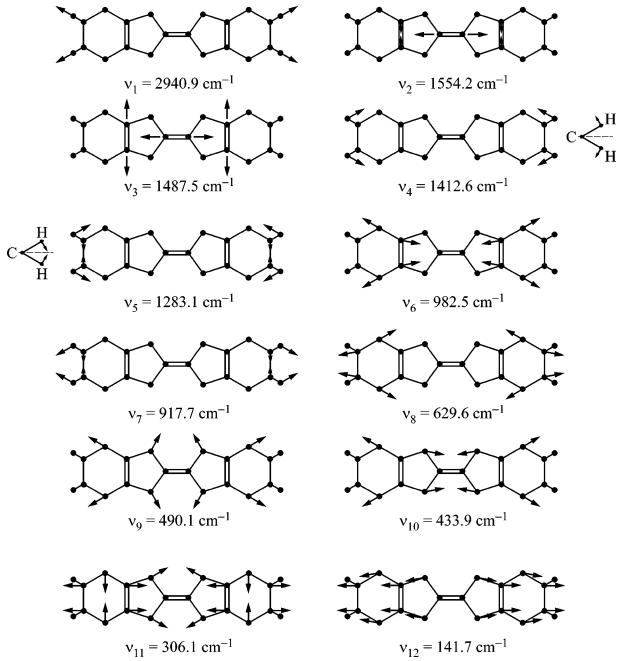

Figure 10. Atomic displacement vectors and frequencies for the 12 totally symmetric A_g modes of neutral BEDT-TTF, calculated by J. Eldridge et al.[62] All of the vectors are in the molecular plane, except the out-of-plane C−H bends in ν_4 and ν_5, which are indicated (adapted with permission from ref 60).

Most important in the present context, all groups agree on the assignment of the bands which involve vibrations of the central and ring C=C double bonds: $\nu_2(A_g)$ and $\nu_3(A_g)$ in D_{2h} notations. Because, out of the A_g modes, they are the ones most sensitive to the change of coupling, e.g., symmetry changes in the structure, in the following sections we will focus mostly on the information obtained from the analysis of these two modes.

As an example, the infrared reflection measurements on κ-(BEDT-TTF)$_2$Cu[N(CN)$_2$]Br are presented in Figure 11. The most intensive mode in the optical conductivity is $\nu_3(A_g)$, which has the largest coupling constant. For the natural compound κ-(BEDT-TTF)$_2$Cu[N(CN)$_2$]Br, the $\nu_5(A_g)$ mode appears as an antiresonance in the wide band which belongs to the $\nu_3(A_g)$ mode; these two modes are observed as separate peaks in isotope-substituted compounds for which the $\nu_3(A_g)$ mode is moved to lower frequencies.

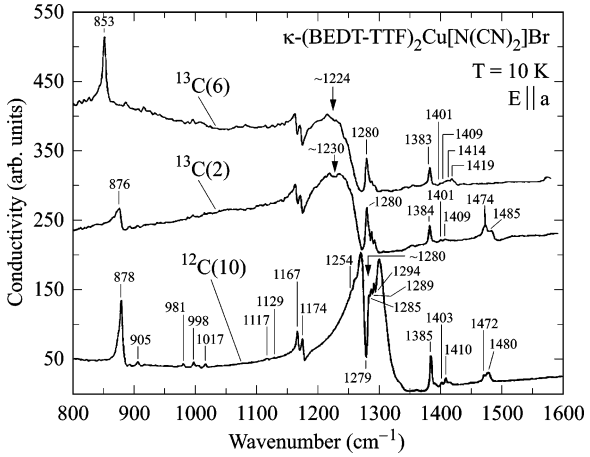

Figure 11. The optical conductivity of (BEDT-TTF)$_2$Cu-[N(CN)$_2$]Br for $E \parallel a$ obtained from the 10 K reflectivity. The spectrum indicated by ^{12}C is measured on molecules with natural isotopes, while for the ^{13}C(2) and the ^{13}C(6) curve the two central carbon and all six carbon atoms, respectively, were substituted by ^{13}C. The ^{13}C spectra have been offset for clarity. (Reprinted with permission from ref 60. Copyright 1996 Elsevier B. V.)

We obtain $\nu_3(A_g) = 1224$, 1230, and ~1280 cm^{-1} for ^{13}C(6), ^{13}C(2), and the natural ^{12}C(10), respectively; and accordingly $\nu_5(A_g) = 1280$, 1280, and ~1279 cm^{-1}. The vibrational features in the infrared spectra of organic conductors are normally shifted to lower frequencies compared to their Raman modes because they are activated by EMV-coupling; the difference increases with the coupling constant. The eigenvectors of the observed vibrational modes might be changed for molecules in the conducting solid, as shown in ref 59 for the example of $\nu_2(A_g)$ and $\nu_3(A_g)$ modes.

3.3. Probing the Charge on the Molecule

The analysis of the BEDT-TTF intramolecular vibrations yields the fact that the position of some modes depends on the charge located on the molecule. H. H. Wang et al.[65,66] performed a systematic study of the room temperature Raman scattering on various BEDT-TTF salts in different oxidation states, which was confirmed and completed by Yamamoto et al.[67] The $\nu_2(A_g)$ and $\nu_3(A_g)$ but also the $\nu_6(A_g)$ modes show a significant shift to lower frequencies as the charge per BEDT-TTF molecule changes from neutral to $+e$ or even $+2e$. As plotted in Figure 12 the slope is approximately -80 to -100 cm$^{-1}/e$ for the $\nu_2(A_g)$ and $\nu_3(A_g)$ vibrations and only -26 cm$^{-1}/e$ for the $\nu_6(A_g)$ mode.[65−67] A similar conclusion was drawn by O. Drozdova et al.[68] for BEDO-TTF salts. In the room temperature Raman spectra of most of these 1:2 compounds, the band show positions indicating a charge $+0.5e$ per molecule in agreement with structural data. In the infrared spectra, they are even more shifted due to EMV-coupling (see previous Section 3.2).

The infrared active $\nu_{27}(B_{1u})$ vibration is the out-of-phase contraction of the C=C double bonds in the BEDT-TTF rings, which leads to a dipole-moment change parallel to the long axis of BEDT-TTF molecule (cf. Figure 21 below). It can be observed

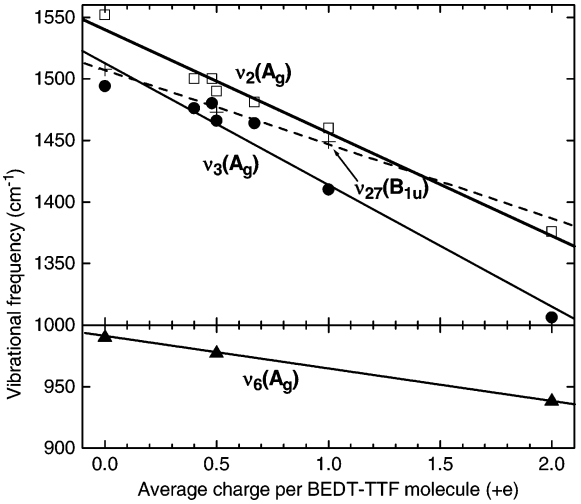

Figure 12. Infrared frequencies of $\nu_{27}(B_{1u})$ mode and Raman shift of $\nu_2(A_g)$, $\nu_3(A_g)$, and $\nu_6(A_g)$ modes for various BEDT-TTF molecules in different oxidation states (data taken from refs 65−67 and 70).

perpendicular to the highly conducting plane of BEDT-TTF crystals,[69] in powder pellets, or on the symmetry breaking in Raman scattering. Upon change of the BEDT-TTF valence, the mode moves by -59 cm$^{-1}/e$ as reported by J. Moldenhauer et al.[70]

Interestingly, the shifts of these vibrational lines are more or less identical for all the crystallographic phases since they are based on intramolecular vibrations which involve the central C=C bonds. Thus, observations of the vibrational frequencies in the infrared and Raman spectra can be utilized to detect the actual charge located on the molecule.[65,70] It was first demonstrated by J. Moldenhauer et al.[70] and subsequently by other groups[67] that in fact the frequencies of those modes which involve C=C vibrations are sensitive to the charge population on the molecule and split upon passing through a charge-order transition. We will discuss this in detail in Section 4.5 below.

It is well-known that a distortion of the unit cell reduces the local symmetry and lifts phonon degeneracies, the nature of the multiplet splitting in the infrared providing information on how the degeneracy is removed. In organic conductors the EMV-coupled A_g modes serve as especially sensitive indicators for changes of the crystal structure through a phase transition. In the case of a symmetry break due to structural effects, the central C=C vibrational band splits. This was nicely followed by S. Baker et al.[71] for different phases of (BEDT-TTF)$_3$(ReO$_4$)$_2$.

4. Interplay between Structural and Electronic Properties

4.1. Structural Arrangements

The two-dimensional synthetic metals discussed in this review consist of organic donor molecules such as BEDT-TTF $^{+0.5}$ or BEDO-TTF$^{+0.5}$ packed in layers and separated by sheets of acceptor molecules. The anions mainly serve as spacers and charge reservoir; the electronic transport solely takes place in the donor layers, where the overlapping HOMO orbitals

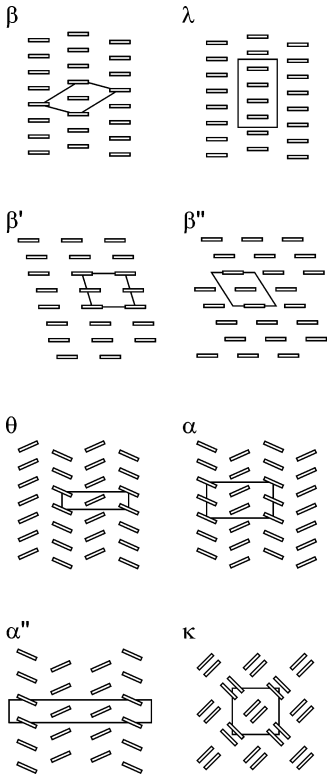

Figure 13. Different stacking patterns found in BEDT-TTF salts: in the β and λ arrangement the molecules are normal to the stacks, for the β' and β'' phases the stacking direction is slightly tilted, the θ and α phases consist of two different stacks within which the molecules have opposite tilt angles, in the α'' phase two stacks have the molecules tilted in one direction, two in the opposite direction, and the κ-phase pattern consists of dimers oriented normal to each other.

of the adjacent molecules form a conductance band. In good approximation the organic molecules are planar (cf. Section 3.2) with their long axes roughly normal to the conduction plane.

The arrangement of the donor molecules within the planes is crucial for the orbital overlap which determines the hopping integral t (or in other words the bandwidth W); it also influences the shape of the Fermi surface. Thus, most of the electronic properties are determined by the packing pattern of the organic layer. The various stacking arrangements found in these radical cation salts are labeled by Greek letters based on historical reasons. Some of the patterns are sketched in Figure 13; a more detailed discussion can be found in refs 9 and 72−74. The simplest order are parallel stacks of the BEDT-TTF ions with the molecular plane perpendicular to the stacking axis. The organic molecules can have equal distance within the stacks (β-phase), or the distances alter slightly leading to a distinct dimerization, as in the case of the λ-pattern. The molecule planes can be tilted in different ways with respect to the stacking direction as is observed, for example, in β''-phase and θ-phase. In this arrangement, there might also be a dimerization because neighboring molecules are tilted in a slightly different fashion and have alternating distances, which is found, for instance, in the α-phase. In contrast to those patterns that exhibit some sort of stacks, the κ-phase has an arrangement of two molecules facing each other, while the neighboring pairs are rotated perpendicular to it.

Due to the layered structure of these compounds, the conductivity and reflectivity perpendicular to the layers are low and only weakly frequency dependent, as typical for an insulator, while the in-plane properties resemble those of a metal. Naturally, the in-plane optical properties of the organic conductors depend significantly upon the structure of the conducting layer. We can identify some simple correlations between the crystallographic arrangement of the BEDT-TTF molecules and their reflectivity spectra. For compounds with stacked BEDT-TTF molecules, the in-plane main optical axes are commonly found parallel and perpendicular to the stacks. The higher reflectivity, plasma frequency, and optical conductivity are observed perpendicular to the stacks (e.g., the β-phase in Figure 6) because the patterns show a larger overlap of the neighboring molecular orbitals in this direction. On the other hand, a higher intensity of the EMV-coupled features is generally observed in the polarization parallel to the stacks, where the neighboring molecules face each other. The degree of dimerization of the molecules in the structure correlates with the intensity of the wide mid-infrared band, which is commonly assigned to interband transitions,[29] and with the strength of EMV-coupling. The spectra of the most dimerized κ-phase always show a pronounced mid-infrared band and very intensive vibrational features (cf. Figure 7).[32]

4.2. Band Filling versus Electronic-Correlation Effects

Changing the packing pattern of the molecules alters the width of the conductance band which is typically of about 1 eV. A "fine-tuning" is achieved by changing the chemical composition of the anion, when atoms of different size but same valence are varied. The resulting small variation of t is often called "chemical pressure" (positive or negative) because similar effects can be reached by applying external "physical pressure" (hydrostatic or uniaxial).

The physical properties of two-dimensional conductors not only depend on the packing pattern and the size of transfer integral t related to it; the on-site and intersite Coulomb interactions U and V between the carriers are other crucial parameters.[36,75] The on-site Coulomb repulsion can be estimated from the difference between the first and the second oxidation potential, i.e., the electron affinity, which can be determined by photoelectron spectroscopy or cyclic voltammetry measurements;[76,77] for BEDT-TTF molecule a value of 0.5 eV for the effective U, which is a balance of on-site and intersite electron−electron interaction, was obtained. This is in agreement with the estimation of this value from the optical spectra (e.g., ref 53) and with the theoretical prediction of ref 75, where a detailed discussion of obtaining the values of electronic correlations is carried out. On-site Coulomb energy increases on going from BEDT-TTF and TMTSF to TMTTF and to TTF, while it does not change substantially when going to BEDO-TTF[78] or BETS. Important for transport and optical properties, however, is the ratio of the interaction strength

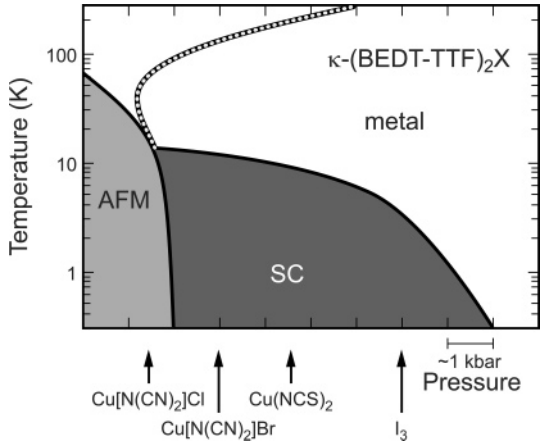

Figure 14. Phase diagram of different κ-phase salts of BEDT-TTF. At ambient pressure (BEDT-TTF)$_2$Cu[N(CN)$_2$]-Cl is insulating at low temperatures, while (BEDT-TTF)$_2$Cu-[N(CN)$_2$]Br and (BEDT-TTF)$_2$Cu(NCS)$_2$ become superconducting. Applying hydrostatic pressure of less than 1 kbar on κ-(BEDT-TTF)$_2$Cu[N(CN)$_2$]Cl, the same ground state can be reached as by substitution of Cl by Br. κ-(BEDT-TTF)$_2$I$_3$ becomes superconducting at $T_c \approx 3$ K.

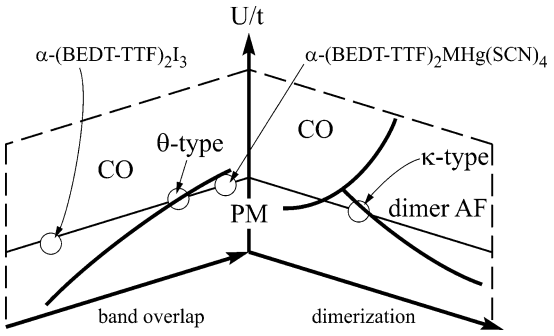

Figure 15. Schematic phase diagrams for the unified view of (BEDT-TTF)$_2X$ for $V/U \approx 0.25$. PM, CO, and dimer AF denotes the paramagnetic metallic, charge-ordered and dimeric antiferromagnetic phases, respectively. (Reprinted with permission from ref 80. Copyright 2000 Physical Society of Japan.)

to the size of the transfer integral (or width of the conductance band): U/t and V/t. Apparently, these parameters can be changed by variation of the orbital overlap, i.e., by substitution of donor molecules or by substitution at the anion side.

The fact that bandwidth and Coulomb repulsion are of the same order of magnitude already suggests electron−electron interactions. The influence of electronic correlation is demonstrated at the phase diagram (Figure 14) obtained for the κ-phase salts over the years.[36] The ground state of these compounds changes from an antiferromagnetic insulator to a superconductor and eventually to a metal by applying physical pressure or chemical pressure, i.e., by variation of the anion molecules. In a more general way, Kino and Fukuyama[79] and subsequently Seo[80] proposed a phase diagram that shows the dependence of different insulating ground states on U/t for the α, θ, and κ stacking patterns (Figure 15).

A most efficient way to control physical properties of materials is known to be the change of band filling, i.e., the shift of the Fermi level. It was used in many different types of compounds, for example, in the case of high-temperature superconductors built on CuO perovskites, superconductivity is reached by doping of the parent compound La_2CuO_4 in the way that La^{3+} is substituted by Sr^{2+}, and by excess oxygen doping. The antiferromagnetic, insulating behavior is suppressed and eventually the superconducting state appears. By a similar doping mechanism the fullerenes A_xC_{60} (A = alkali metal and $\approx$3) become superconducting. An elegant alternative would be the external control of the band filling of inorganic or organic solids by utilizing a field-effect arrangement; at present it remains a challenge.

The approach to control the band filling is rarely used for the quasi-two-dimensional organic conductors because the substitution of a counterion with a different charge usually results in a change of the crystal structure or even stoichiometry. Most often the (BEDT-TTF)$_2X$ compounds exhibit a three-quarter-filled conduction band (having on average $+0.5e$ per molecule), corresponding to a quarter-filled hole-band. The dimerization of the organic molecules, most pronounced in the case of the κ-phase, splits the conduction band and an effectively half-filled band remains, having $+1e$ per dimer. Within the family of charge transfer salts, there are only a few examples of compounds with a band filling different from 1/4 and 1/2. Compared to BEDT-TTF salts, it seems that BEDO-TTF-based conductors are more suitable to vary the band filling, as they mostly form a β''-structure which appears less dependent on the anions.

A particular challenge seem to be the synthesis of organic conductors whose electronic ground states can be controlled by systematic carrier doping. In the case of the one-dimensional (Me$_2$DCNQI)$_2$Li$_{1-x}$Cu$_x$ salts, the charge concentration was varied by gradual substitution of the anions. In a comprehensive study,[81] the change of the dc-transport from a metal to an insulator was investigated when getting from 1/2 to zero-filling of the conductance band; also the optical properties have been measured. Recently, H. Mori et al.[82] succeeded to gradually control the band filling of the two-dimensional system (BEDT-TTF)$_y$GaCl$_4$ (with y = 2 and 3) by partially substitution of $(GaCl_4)^-$ by $(CoCl_4)^{2-}$ in an anion block sheet. DC resistivity measurements have been carried out on different phases of (BEDT-TTF)$_y$(GaCl$_4$)$_x$(CoCl$_4$)$_{1-x}$ to characterize the system. Other, more advanced experiments are still missing; optical investigation have failed so far due to the limited sample size.

4.3. Fingerprints of Electronic Correlations

Electronic correlations are known to strongly influence the shape of the spectra in the region of intraband excitations; they have been widely studied in the field of heavy fermions.[1,83] In the simplest picture, electron−electron interaction leads to an enhancement of the effective mass m^* accompanied by a decrease of the scattering rate $1/\tau^*$. According to eq 7, the spectral weight of the intraband transitions decreases

$$\int_0^{\omega_c} \sigma_1(\omega)\, \mathrm{d}\omega = \frac{\pi N e^2}{2m^*} \qquad (27)$$

although the dc conductivity $\sigma_{dc} = Ne^2\tau^*/m^*$ remains unchanged. An estimate of the effective electron mass m^* of the organic conductors using a variety of methods (e.g., de Haas-van Alphen oscillations[84]) yields values of about 1.5−5 m_e, depending on the compound; in any case, electron−electron correlations may not be neglected in low-dimensional synthetic metals. In the optical spectra of organic solids, the observed Drude peak is often very narrow. For example, at $T = 10$ K for the κ-(BEDT-TTF)$_2X$[32] and for some α-phase compounds,[85] an effective mass $m^* \approx 2m_e$ is obtained from optical results.

Correlation effects surface in different ways in the optical spectra of synthetic metals, depending whether the conduction band is half-filled, quarter-filled, or contains other filling values. In the following, we present examples for all of these cases.

4.3.1. κ-(BEDT-TTF)$_2X$

Out of the organic metals with half-filled conduction band, the κ-phase compounds, which are fully dimerized (Figure 13), are certainly the most studied ones.[31−34,69,86−93] As an example, the optical reflectivity $R(\omega)$ and conductivity $\sigma(\omega)$ of the superconductor (BEDT-TTF)$_2$Cu(NCS)$_2$ are plotted in Figure 7. The room temperature spectra of all these compounds are characterized by a broad mid-infrared band with a maximum at about 2500−3000 cm^{-1}, commonly assigned to the interband transitions,[32] and by the absence of a Drude component, although the crystals are highly conducting in the plane. For the superconducting compounds, a narrow Drude-like peak appears in the optical conductivity as the temperature is reduced below 50 K (but still in metallic phase). The width of the low-temperature conductivity peak at zero frequency is only about 40 cm^{-1} for κ-(BEDT-TTF)$_2$Cu(NCS)$_2$ and of similar values for the other superconducting compounds of the κ-phase.[33] The low-frequency spectral weight grows on the expense of the mid-infrared spectral weight to some extent: the intensity of the mid-infrared maximum decreases as the temperature is lowered.[32,33] However, a growth of the total spectral weight by a factor of about 1.5 is observed for these compounds,[31] which is one of the fingerprints of strong electron−electronic correlations. The frequency of the mid-infrared maximum does not significantly change with temperature for κ-(BEDT-TTF)$_2$Cu[N(CN)$_2$]Br,[33] while for κ-(BEDT-TTF)$_2$Cu(NCS)$_2$ the maximum in the b-direction shifts up by 700 cm^{-1} when cooling to $T = 12$ K.[31] In contrast to those superconducting compounds, in κ-(BEDT-TTF)$_2$Cu[N(CN)$_2$]Cl the spectral weight moves to higher frequencies and an optical gap gradually opens around 900 cm^{-1} [89] upon cooling below 50 K. Since there are no changes in the vibrational features, no symmetry (structural) change occurs at this phase transition to an insulating state.

Dynamical mean-field-theory calculations[94] on a frustrated two-dimensional lattice at half-filling with strong on-site Coulomb repulsion $U \approx W$ (with $W = 8t$ being the bandwidth for the two-dimensional case) were successfully applied to the κ-type compounds. In that case, the optical conductivity exhibits a Drude peak at low temperatures,

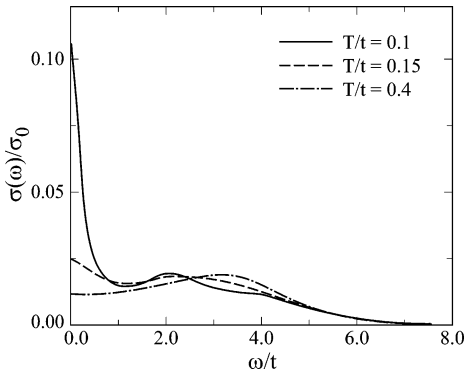

Figure 16. Frequency dependence of the normalized conductivity $\sigma(\omega)/\sigma_0$ for different temperatures. The curves are shown for $U = 4t$ and a diagonal hopping integral of $0.1t$. The feature around $\omega = U/2$ is due to transitions from the coherent quasi-particle band at the Fermi energy to the upper Hubbard band and from the lower Hubbard band to the quasi-particle band. The broad feature at $\omega = U$ at higher temperatures is due to transitions from the lower to the upper Hubbard band. The Drude response shows up only at low temperatures. Note that most of the spectral weight is contained in the high-frequency features. (Reprinted with permission from ref 37. Copyright 2000 American Physical Society.)

which is suppressed for $T > 50$ K because close to a Mott metal−insulator transition the quasi-particles are destroyed[31,36] as displayed in Figure 16. For large values of U/t the half-filled system becomes a Mott−Hubbard insulator. This type of phase transition is observed for κ-(BEDT-TTF)$_2$Cu[N(CN)$_2$]Cl below 50 K, as shown by the antiferromagnetic phase in Figure 14. In agreement with the theory, the application of some external pressure shifts the (BEDT-TTF)$_2$Cu[N(CN)$_2$]Cl compound across the phase boundary: it remains metallic and even undergoes a superconducting transitions at a critical temperature as high as 13 K.

4.3.2. (BEDT-TTF)$_4$[Ni(dto)$_2$]

The first evidence of a pseudogap in the electronic spectra of a two-dimensional organic metal due to electronic correlations was reported for (BEDT-TTF)$_4$[Ni(dto)$_2$];[95,96] a two-dimensional metal which, however, does not become superconducting down to 0.06 K.[97] The structure of its conducting layer resembles the β-arrangement of the organic molecules.

It can be seen in the optical spectra plotted in Figure 17 that as the temperature is reduced below 150 K a dip develops in $R(\omega)$ with a corresponding mode in $\sigma(\omega)$ around 200 cm^{-1}. This feature is ascribed to excitations across a gap caused by correlation effects. The position of the maximum in the optical conductivity is the same for both axes and does not change with temperature. The intensity (oscillator strength) of this feature increases linearly by about a factor of 10, when going from 150 to 50 K, and stays constant below. At reduced temperatures ($T < 50$ K) a narrow Drude-like peak grows below this gap containing only 2 to 4% of the spectral weight. The feature in $\sigma(\omega)$ at 200 cm^{-1} is interpreted as a precursor effect that appears in a metallic state in the proximity of a quantum phase transition which partially or totally gaps the Fermi surface. As we

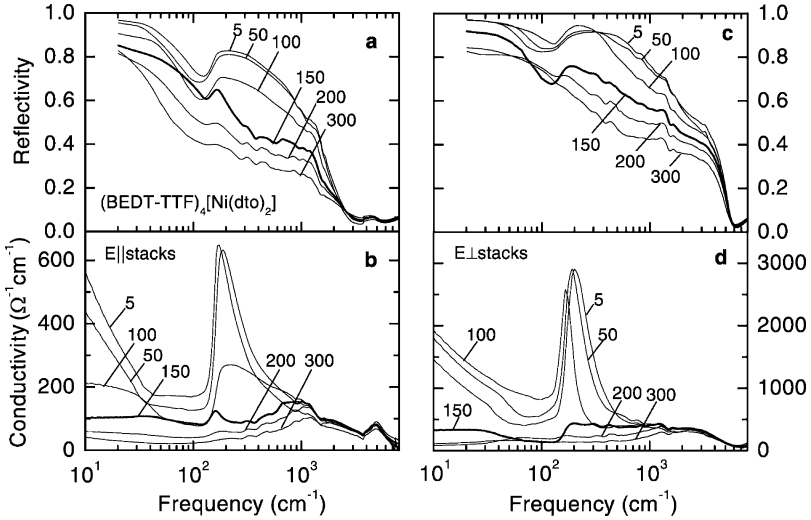

Figure 17. (a) Frequency dependent reflectivity $R(\omega)$ and (b) optical conductivity $\sigma(\omega)$ parallel to the stacks of (BEDT-TTF)$_4$[Ni(dto)$_2$] for different temperatures as indicated. Panels (c) and (d) show the reflectivity and conductivity, respectively, measured perpendicular to the stacking direction for different temperatures. In both orientations, a gap-feature is clearly seen at around 200 cm^{-1}. (Reprinted with permission from ref 95. Copyright 2000 American Physical Society.)

approach the transition (by changing the relevant microscopic parameters) spectral weight is transferred from the Drude response to frequencies above the charge gap.[95]

The unit-cell of (BEDT-TTF)$_4$[Ni(dto)$_2$] contains four BEDT-TTF$^{+0.5}$ molecules which are dimerized along the stacks. Band structure calculations reveal two conduction bands, each accommodating one hole, i.e., half-filling.[97] Correlation effects are taken into account with a Hubbard U-term, which sets an energy cost U for doubly occupied orbitals. Since we have precisely one hole per orbital, large values of U would lead to the localization of holes and hence a Mott insulating state. While the antiferromagnetic insulating phase of the κ-phase salts is described if one chooses $U > U_c$, for the present material $U < U_c$. Thus, the system remains metallic at arbitrary temperatures and no phase transition is present. The fact that only a few percent of the total spectral weight of the optical conductivity is contained in the narrow Drude-like mode indicates a mass enhancement due to proximity of the Mott transition, taking into account the large Fermi surface measured by quantum oscillations.[97]

The electronic phase diagram of a half-filled metal is mainly determined by the on-site repulsion U. While in one dimension an electron gas becomes insulating for any small U,[98,99] a two-dimensional electron system remains metallic as long as $U < U_c$, some critical value, with a distinct temperature dependence as described above.[37,38] Quarter-filled compounds on the other hand are known to stay metallic for all values of on-site repulsion U. However, the large values of both U and nearest-neighbor repulsion V can lead to an insulating ground state due to charge ordering,[94,100] as discussed in the following section.

4.4. Charge Ordering

During the past decade, charge-order phenomena have attracted considerable interest in the field of both organic conductors and transition metal oxides. Due to the modification of some external parameter, such as the temperature, pressure, or magnetic field, the charge distribution undergoes appreciable changes, which can be observed in a number of physical properties. The classical example is the Verwey transition in magnetite Fe_3O_4 at $T_{CO} = 120$ K.[101] More recently, the importance of charge-order phenomenon was revealed in a number of perovskites for which the Coulomb interaction is known to play a crucial role.[102,103] The phenomena of colossal magnetoresistance in manganites[104,105] is an example of enormous impact. The stripe formation in the two-dimensional nickelates and the high-temperature superconducting cuprates[106−108] is another intriguing topic in this regard.

Although first indications were around for many years, only very recently charge ordering was unambiguously proven in the quasi-two-dimensional organic conductors of the BEDT-TTF family and related salts. From the angular dependence of the g-factor measured by ESR spectroscopy on θ-(BEDT-TTF)$_2$CsZn(SCN)$_4$ a change of the electronic nature and symmetry due to charge ordering was concluded.[109] More clearly, NMR measurements revealed the existence of charge disproportionation among the BEDT-TTF molecules, first in θ-phase compounds[110] and next in α-(BEDT-TTF)$_2$I$_3$.[111]

Charge order or charge separation describes the fact that the organic donor molecules D do not homogeneously carry half an elementary charge, as suggested by stoichiometry, for instance, but the charge is distributed unequally. The disproportionation δ of charges takes place like $D^{0.5+\delta}D^{0.5-\delta}D^{0.5+\delta}D^{0.5-\delta}$ or in the extreme case ($\delta = 0.5$) $D^+D^0D^+D^0$. As sketched in Figure 18, the charge disproportionation may be accompanied by some dimerization or structural ordering. The charge-ordered state becomes a Wigner crystal in its limiting case. It also resembles the $4k_F$ charge-density-wave state; however, even in quasi-two-dimensional compounds the charge density wave is still induced by Fermi-surface nesting[2] and thus requires a presence

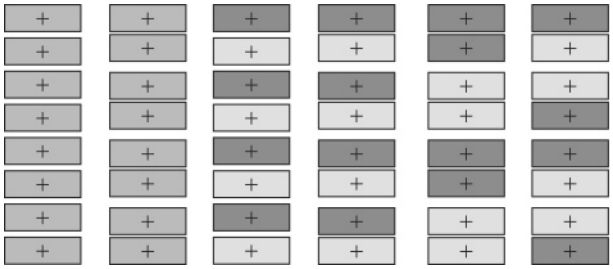

Figure 18. Possible arrangement of the molecules along the stacks. The disproportionation of charge is depicted by the different gray shade. The molecules can be dimerized, too, which may or may not be accompanied by charge disproportionation. The periodicity doubles if neighboring dimers carry different charge but also if charge-rich molecules in adjacent dimers form pairs.

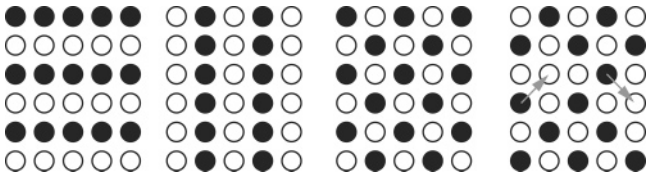

Figure 19. Charge ordering in two dimensions can lead to horizontal (perpendicular to the stacks), vertical (parallel to the stacks), and diagonal stripes. The periodicity depends on the band filling; the examples are shown for quarter-filled bands. If the band-filling deviates from 1/4, vacancies in the pattern encourage hopping, leading to an enhanced dc conductivity.

of one-dimensional parts. Whereas the charge order does in principle not dependent on the Fermi surface and its dimensionality, it is primarily produced by the intersite Coulomb interaction V, at least for the quarter-filled case. Accordingly, charge-ordered states are essentially paramagnetic, in contrast to the charge-density-wave state which usually is nonmagnetic. In general, however, the spatial distribution can be different for spin up and spin down, leading to a spin polarization.

In general, the two-dimensional organic conductors cannot be mapped on a simple square lattice since there is a preferred direction due to the stacks. Depending on the arrangement of the organic donors in the conducting plane, the distance and the angle of the molecules with respect to each other the transfer integrals parallel and perpendicular the stacks are different.[80,112] The charge-rich and charge-poor site can arrange themselves perpendicular to the stacks, parallel to the stacks, or diagonally. Accordingly horizontal, vertical, or diagonal stripes can occur, as sketched in Figure 19.

Within the Hartree mean-field approximation for the extended Hubbard model Fukuyama, Kino[79] and Seo[80] investigated charge-order phenomena in quasi-two-dimensional quarter-filled organic compounds (BEDT-TTF)$_2X$ taking into account on-site repulsion U and intersite Coulomb interaction V:

$$H = t\sum_i c_i^\dagger c_{i+1} + U\sum_{i\sigma} n_{i\sigma} n_{i\bar{\sigma}} + V\sum_i n_i n_{i+1} \quad (28)$$

where t represents the nearest neighbor hopping integral. Using slave bosons, M. Calandra et al.[113] further explored the metal−insulator transition in a quarter-filled extended Hubbard model. For U, $V \gg t$ the ground state is insulating with checkerboard charge order and long-range antiferromagnetic correlations along the diagonals.[114] Looking at the metallic phase (finite U/t) close to the charge-order transition in more detail, J. Merino et al.[100] calculated the dynamical properties of an extended Hubbard model relevant for quarter-filled layered molecular crystal using Lanczos diagonalization technique. A transition from a metallic phase to a charge-ordered phase occurs as the ratio of the nearest-neighbor Coulomb repulsion V to the hopping integral t increases beyond some critical value. As the system approaches the charge-order transition, the Drude weight decreases continuously and the electronic system eventually becomes insulating. Still on the metallic side, the charge-correlation function exhibits a plasmon-like mode which increases in strength and softens as the system is driven closer to the charge-order transition. These calculations agree perfectly with optical results obtained in metallic θ-phase compounds,[30,115] β''-phase system,[39] and α-salts.[85] In the latter compound, it was observed that the spectral weight of the Drude contribution is suppressed, while the optical weight around 500 to 1000 cm^{-1} increases at low temperatures.

Upon passing through a charge-order transition, significant changes in the electrodynamic properties are observed at low frequencies: the Drude contribution to the optical response vanishes, and the spectrum becomes semiconductor-like.[30] The actual charge pattern of horizontal, vertical, or diagonal stripes (Figure 19) very much depends on the parameters of the models. The intramolecular vibrations of BEDT-TTF molecules—both the Raman active A_g modes and the same in infrared spectra activated by EMV-coupling—can be used to follow the charge disproportionation: the position of $\nu_2(A_g)$ and $\nu_3(A_g)$ bands is approximately proportional to the charge on the BEDT-TTF molecule (Figure 12), while the symmetry analysis of the vibrational bands yields information on the charge-order pattern.[67]

A deviation from a quarter-filled system results in a strong increase of the spectral weight of the Drude term, since the checkerboard pattern is not complete. For any value of V there are unoccupied sites, which make dc transport possible (Figure 19).[116]

4.5. Metal-to-Insulator Transition Due to Charge Ordering

A complete charge-order causes the localization of the conduction electrons, which implies a metal-to-insulator transition. In contrast to a charge density wave, the driving force is the Coulomb repulsion U and V. The metal−insulator transition is purely electronic and thus not determined by a structural distortion, although a slight rearrangement of the underlying lattice is commonly detected. At present, it is not clear how important these accompanying structural transitions are. In several cases it seems that charge order gradually develops as the temperature is reduced, and only when the symmetry break in the lattice occurs, the physical properties change dramatically. Theoretical investigations[117,118] suggest

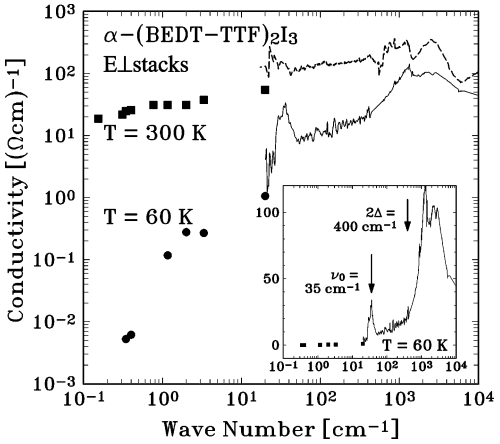

Figure 20. Frequency-dependent conductivity of α-(BEDT-TTF)$_2$I$_3$ perpendicular to the stacks at $T = 60$ K (solid line) and $T = 300$ K (dashed line). The solid squares and circles are obtained by microwave cavity experiments at various frequencies and quasi-optical reflection measurements at the corresponding temperatures. The inset enhances the energy gap at 400 cm^{-1}. (Reproduced with permission from ref 119. Copyright 1994 EDP Sciences.)

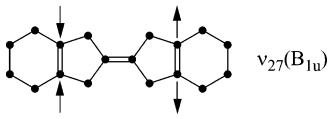

Figure 21. Sketch of the atomic displacement vectors for the infrared active $\nu_{27}(B_{1u})$ mode which induces a charge flow along the molecular axis.

that charge order is accompanied by cooperative bond dimerizations or even tetramerization. The charge-order phase transition is of second order. Commonly fluctuations and indications of ordering phenomena can be found well above the actual transition temperature.

4.5.1. α-(BEDT-TTF)$_2$I$_3$

The most prominent example of a complete metal-to-insulator transition due to charge order happens in α-(BEDT-TTF)$_2$I$_3$ where a sudden drop of the conductivity $\sigma(T)$ by orders of magnitude is observed at $T_{MI} = 135$ K. Figure 20 shows the optical conductivity $\sigma(\omega)$ in a very broad spectral range for two different temperatures above and below the metal-to-insulator transition, respectively.[119] As $T < T_{MI}$, a gap-like feature opens at 400 cm^{-1} due to the charge localization. The charge transport takes place by some incoherent hopping mechanism being slightly larger along the *b*-direction perpendicular to the stacks. A peak around 35 cm^{-1} which shows up in both polarizations might be assigned to an external vibration of the entire BEDT-TTF molecule.[120]

The infrared absorption spectra taken on α-(BEDT-TTF)$_2$I$_3$ powder at different temperatures[70] are displayed in Figure 22. Due to charge disproportionation, two new bands emerge at the metal−insulator phase transition T_{MI} which are arranged symmetrically around the C=C stretching mode $\nu_{27}(B_{1u})$ at 1477 cm^{-1}; this principal vibrational feature remains present below the phase transition. According to Figure 12, the frequencies of the $\nu_{27}(B_{1u})$ modes allow us to evaluate the average charge per donor molecule: +0.15*e*, +0.52*e*, and +0.9*e*. This implies that a charge localization takes place in two crystallographically different molecules, while the others maintain an average charge of about + *e*/2. As pointed out by M. Meneghetti et al.[44] based on polarized infrared reflection measurements, the symmetry of the high-temperature phase is not conserved into the low-temperature phase. While for $T > T_{MI}$ the A and A′ molecules in stack 1 are connected by an inversion center, this inversion symmetry disappears in the insulating phase ($T < T_{MI}$), and both sites are not equivalent any more (cf. Figure 8). Recent and very detailed Raman scattering experiments by R. Wojciechowski et al.[121] confirm these findings. The splitting of the $\nu_2(A_g)$ mode yields an average charge-disproportionation ratio of +0.2*e*/+0.8*e*, i.e., $\delta = 0.3$. The charge is ordered in horizontal stripes perpendicular to the stacks, with the A and B sites being charge rich and A′ and C donor molecues being charge-poor sites. Already above the metal-to-insulator transition small deviations of $\delta_M = 0.05e$ from the uniform charge distribution are found.

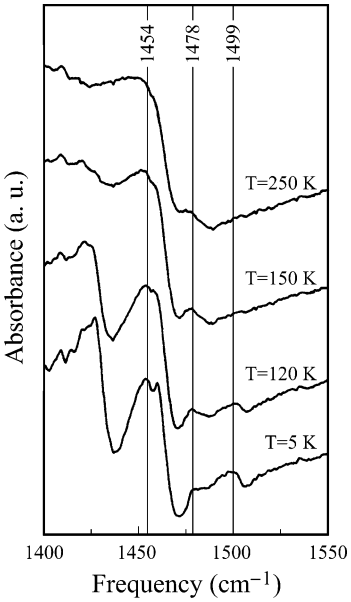

Figure 22. Optical absorption of α-(BEDT-TTF)$_2$I$_3$ at different temperatures. The splitting of the $\nu_{27}(B_{1u})$ mode is indicated (data taken with permission from ref 70).

The results of the vibrational spectroscopy were in part confirmed by magnetic measurements. The splitting of the ^{13}C NMR resonance peak observed below T_{MI} is ascribed to the emergence of more than one kind of BEDT-TTF molecule with different valence.[111] Comparing the temperature dependence of the shift of the charge-rich site with that of the susceptibility, it was concluded that the charge disproportionation is nearly perfect (+*e*:0). Angle-dependent measurements of the line shape infer vaguely that the charge-rich sites are selectively located on the C sites and on half of the A molecules, but not on the B sites. Thus, the charge stripes run along the direction perpendicular to the stacking axis, forming horizontal stripes.[122] Hartree−Fock calculations taking into account only on-site Coulomb interaction *U* predict that charge ordering will occur between the stacks (vertical stripes).[79] However,

when the intersite Coulomb repulsion V and the on-site U is substantially large (cf. Section 4.4), horizontal stripes become stable.[80]

4.5.2.θ-(BEDT-TTF)$_2$MM′(SCN)$_4$

The θ-family has a stacking pattern similar to the α-phase except that the molecules are equal within the stack,[73] i.e., the heringbone arrangement consists of two nondimerized stacks of BEDT-TTF-molecules which are tilted in opposite directions as depicted in Figure 13. During the last years, a fair amount of work was devoted to the systems θ-(BEDT-TTF)$_2$ MM'(SCN)$_4$, which can be modified nicely. Depending on the metal ions M = Rb, Tl, Cs and M' = Zn and Co the dihedral angle between the molecules in adjacent stacks differs slightly, which changes the interchain overlap proportional to the bandwidth.[73,112,123] The systems have quarter-filled hole bands with a two-dimensional closed Fermi surface. Some of the compounds show metallic behavior at room temperature; as they are cooled, however, eventually all members of this family undergo a metal-to-insulator transition at different temperatures. Due to this possibility of tuning the electronic-correlations-to-bandwidth ratio (by substituting the metal ions or applying pressure[123]), systematic investigations of the electronic and vibrational properties of θ-(BEDT-TTF)$_2$$MM'(SCN)_4$ salts have been performed by different groups.[67,30,115]

Two salts of this family, θ-(BEDT-TTF)$_2$RbZn(SCN)$_4$ and θ-(BEDT-TTF)$_2$RbCo(SCN)$_4$, show a sharp metal-to-insulator transition at $T_{MI} \approx 190$ K when cooled slowly (relaxed state); the phase transition is accompanied by a dimerization in the stacks along the c-axis.[123] The polarized reflectance spectra change drastically upon passing through this phase transition (Figure 23). Although the spectra of these salts show no Drude-peak even at room temperature, the low-frequency spectral weight shifts up in frequencies for $T < T_{MI}$ and a gap opens in the optical conductivity spectra around 300 cm^{-1} as was detected for θ-(BEDT-TTF)$_2$RbZn(SCN)$_4$.[115] Using mean-field calculations, H. Tajima et al.[30] assign the mid-infrared band to the transitions between bands which are split due to charge ordering. From this interpretation of the band shape, they concluded that in the insulating phase of θ-(BEDT-TTF)$_2$RbZn(SCN)$_4$ and θ-(BEDT-TTF)$_2$RbCo(SCN)$_4$ the stripes order horizontally, while a charge-order pattern with vertical stripes is present above T_{MI}.

A splitting of vibrational features in infrared reflection and Raman scattering spectra clearly shows the charge disproportionation in the insulating phase of θ-(BEDT-TTF)$_2$RbZn(SCN)$_4$.[67] The Raman modes $\nu_2(A_g)$ and $\nu_3(A_g)$ could be unambiguously identified by isotope substituted molecules. On the basis of the number of peaks of these vibrations observed in the Raman and infrared spectra and with the help of factor-group analysis, K. Yamamoto et al.[67] argue that in this salt horizontal stripes occur in the charge-ordered phase. The splitting of the $\nu_2(A_g)$ vibrations below T_{MI} into two peaks at 1544 and 1480 cm^{-1} allows them to estimate the charge disproportionation of $\delta = 0.35$, assuming a slope of -90 cm$^{-1}/e$ in agreement with Figure 12.

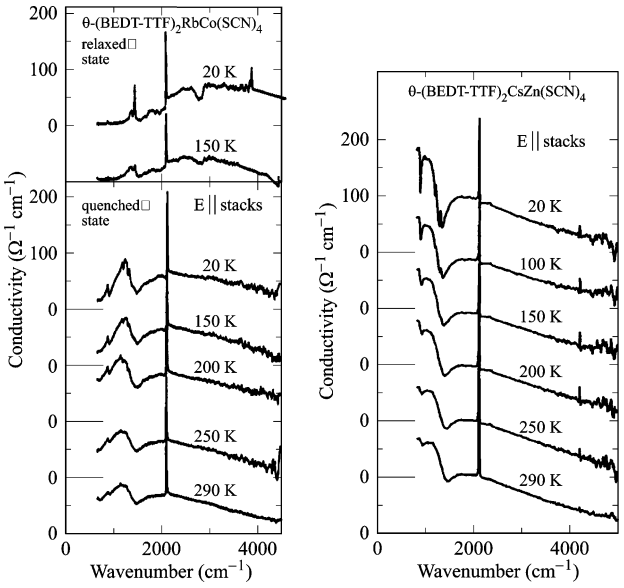

Figure 23. Optical conductivity of θ-(BEDT-TTF)$_2$RbCo(SCN)$_4$ and θ-(BEDT-TTF)$_2$CsZn(SCN)$_4$ measured along the stacks (c-axis) for different temperatures. (Reprinted with permission from ref 30. Copyright 2000 American Physical Society.) While the CsZn compound remains metallic down to 20 K, the RbCo analogue and similarly the RbZn salt do not show a Drude contribution below $T_{MI} \approx 190$ K when cooled rapidly. In the relaxed state, θ-(BEDT-TTF)$_2$RbCo(SCN)$_4$ becomes completely insulating.

Raman scattering experiments were also applied to other compounds of this family to evaluate the charge disproportionation.[124] In θ-(BEDT-TTF)$_2$TlCo(SCN)$_4$ a metal-to-insulator transition due to charge ordering occurs at $T_{MI} \approx 240$ K. The respective splitting of the $\nu_2(A_g)$ and $\nu_3(A_g)$ modes is observed in the Raman spectra and the charge disproportionation is estimated to be $\delta = 0.3$. In θ-(BEDT-TTF)$_2$TlZn(SCN)$_4$, the charge-order transition is observed at $T_{MI} = 165$ K by a drop in the dc conductivity and by splitting of the $\nu_2(A_g)$ mode, leading to the same charge ratio of $+0.2e/+0.8e$. However, a weak $\nu_2(A_g)$ mode of the charge-poor site appears in the spectra already at around 200 K; in the same temperature range a small hump in the resistivity and drop in the low-frequency optical conductivity are observed. The authors suggest that these are indications of charge-order fluctuations, which are observed well above the temperature of phase transition.

As the charge ordering sets in at lower temperatures, a local probe such as ^{13}C NMR spectroscopy shows a splitting of the lines due to the inequivalence of the environment. The ratio of relaxation rate $1/T_1$ of these two lines is very much different (around a factor of 40), which yields a charge disproportionation of approximately ($+0.14e/+0.86e$) [110]. From the temperature dependence of the Knight shift in θ-(BEDT-TTF)$_2$RbZn(SCN)$_4$ T. Takahashi et al.[122,125] estimate a ratio between the charge-poor site and charge-rich site as ($+0.2e/+0.8e$), leading to a charge disproportionation of $\delta = 0.3$. The angular dependence of the line shape infers horizontal stripes along the a-axis, i.e., perpendicular to the stacks. For $T > T_{MI}$ an unusual line broadening is observed, which might indicate some charge disproportionation

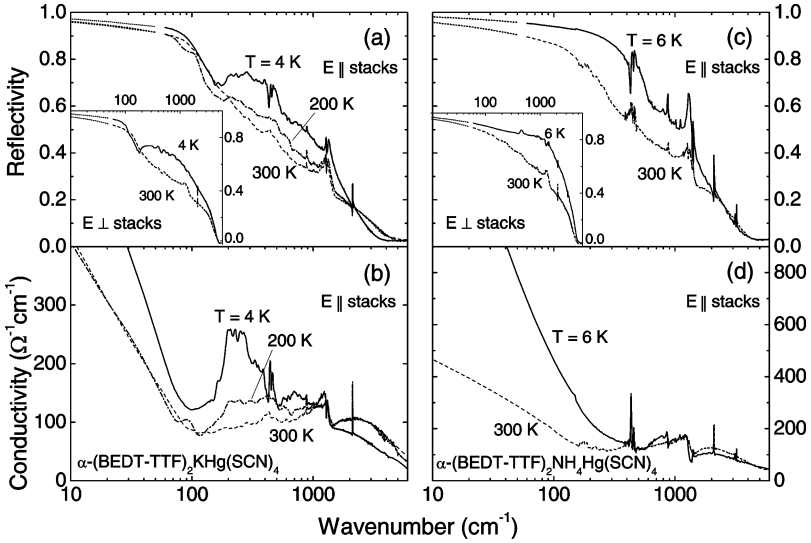

Figure 24. (a) Frequency-dependent reflectivity and (b) optical conductivity of α-(BEDT-TTF)$_2$KHg(SCN)$_4$ for different temperatures as indicated. The panels (c) and (d) show the reflectivity and conductivity, respectively, of α-(BEDT-TTF)$_2$NH$_4$-Hg(SCN)$_4$. The measurements were performed for E parallel to the stacking direction; the E perpendicular to the stacks reflection data are displayed in the corresponding insets. For both polarization the reflectivity of (BEDT-TTF)$_2$KHg(SCN)$_4$ has a dip at around 200 cm^{-1}. (Reprinted with permission from ref 85. Copyright 2003 American Physical Society.)

(without long-range order) even above the insulating state.[122]

In the Cs-analogue θ-(BEDT-TTF)$_2$CsZn(SCN)$_4$ no clear charge separation is detected by NMR.[122] This is in full accordance with the optical behavior as displayed in Figure 23: no significant changes were revealed for $T > 20$ K. The CsZn salt belongs to a uniform phase; it exhibits a broad absorption band around 2000 cm^{-1}, which is attributed to fluctuations of some antiferromagnetic order.[30]

4.6. Close to the Charge-Order Transition

As we have already seen in α-(BEDT-TTF)$_2$I$_3$ and various examples of θ-(BEDT-TTF)$_2$*MM′*(SCN)$_4$, even for temperatures above the metal-to-insulator transition fluctuating charge order might be appreciable although long-range order is still missing. Those fluctuations are typical for second-order phase transitions and are enhanced in reduced dimensions. There is another scenario possible, for which the charge localization is not complete even below the ordering temperature. There might be domains in which stripes are formed due to charge disproportionation, but they are not stable and fluctuate in time and space. Therefore, the conductivity remains metallic, at least partially; nevertheless, fingerprints of the charge order can be revealed in the optical properties.

4.6.1. α-(BEDT-TTF)$_2$MHg(SCN)$_4$

The two-dimensional conducting salts α-(BEDT-TTF)$_2$*M*Hg(SCN)$_4$, where M = K, Rb, Tl, NH$_4$, have attracted considerable attention for various reasons. The NH$_4$ compound is a $T_c = 1$ K superconductor, while the M = K, Rb, and Tl salts remain metallic with indications of a density-wave ground state at $T_p \approx 8$ to 12 K. The Fermi surface calculated for all of these isostructural compounds are almost identical, consisting of two-dimensional closed pockets and quasi-one-dimensional open sheets.[84,126] The conduction band is quarter-filled by holes.

The results of recent optical investigations[85,127] on α-(BEDT-TTF)$_2$*M*Hg(SCN)$_4$ are presented in Figure 24. On cooling of the sample, an overall rise in reflectivity is observed in the M = NH$_4$ salt, but no drastic changes of the general behavior. While at frequencies above approximately 500 cm^{-1} the temperature dependences of all compounds are similar, in the nonsuperconducting salts a new feature in $R(\omega)$ is observed at lower energies: a significant dip in the reflection gradually develops in both polarizations as T drops (Figure 24a) below 200 K, showing up as a maximum in the conductivity spectra $\sigma(\omega)$ slightly above 200 cm^{-1} due to excitations across a pseudogap. It can be pictured as a reduction of the density of states. The position of the peak is the same for both orientations and does not change with temperature.[128] No indications of a pseudogap are found in the NH$_4$ compound.[85,129] In a narrow Drude-like contribution with a scattering rate of less than 30 cm^{-1} remains below the pseudogap. It contains only a few percent of the spectral weight; nevertheless, it is responsible for the dc conductivity and the quantum oscillations.[84] Interestingly, the Drude weight of α-(BEDT-TTF)$_2$NH$_4$Hg(SCN)$_4$ is an order of magnitude larger.

It was suggested that α-(BEDT-TTF)$_2$KHg(SCN)$_4$ is close to a charge-order transition while the NH$_4$ compound is well on the metallic side.[85] The findings were described based on exact diagonalization calculations of the optical conductivity on a quarter-filled extended Hubbard model taking into account both the intrasite Coulomb repulsion U as well as the intersite Coulomb interaction V. For quarter-filled systems, as in the case of the α-phase, Hartree−Fock calculations in a Hubbard model with U = 0.7 eV suggest a paramagnetic metallic ground state for the α-(BEDT-TTF)$_2$KHg(SCN)$_4$.[79] Including the nearest-neighbor interaction V, however, can lead to

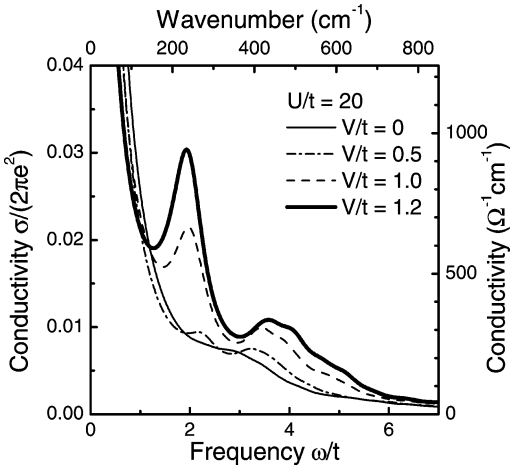

Figure 25. Evolution of optical conductivity as the intersite Coulomb repulsion V/t gradually increases. The results are obtained using exact diagonalization of an extended Hubbard model on a 4×4 square lattice with fixed $U = 20t$. A Lorentzian broadening of $0.4t$ is used for comparison with experimental data. A strong feature develops at low frequencies associated with fluctuations due to short-range charge order. Note that for these values of V the system is on the metallic side of the transition: $V \ll V_c^{MI} \approx 2.2\ t$. The lower and left axes are given in normalized units assuming $a = 1$. For the upper and right axes we used the numerical values ($t = 15$ meV, $a = 10.08$ Å, and $4V_{mol} = 2010$ Å^3) appropriate for α-(BEDT-TTF)$_2M$Hg(SCN)$_4$. (Reprinted with permission from ref 85. Copyright 2003 American Physical Society.)

charge-order phenomena.[80] Exact-diagonalization calculations on an extended Hubbard model at quarter-filling[113] show that a transition from a metal to a checkerboard charge-ordered insulator occurs at $V = V_c^{MI} = 2.2\ t$. Of course, this will lead to a strong redistribution of the spectral weight in the optical conductivity. When the system is insulating the calculated spectrum consists of a single broad resonance centered at $\omega \approx 3\ V$; this corresponds to the energy cost of moving an electron inside the checkerboard. However, for small values of V the checkerboard is not fully formed. As V/t increases, a strong enhancement of the charge correlation function with wavevector $\boldsymbol{q} = (\pi,\pi)$ takes place,[113] signaling the onset of checkerboard charge ordering. Because this is the main effect introduced by V, the low-frequency feature appearing in the calculated optical conductivity can be attributed to the presence of strong charge fluctuations associated with checkerboard charge order in a metallic phase. In Figure 25 $\sigma(\omega)$ is plotted as obtained from calculations on a 4×4 square lattice for $U = 20t$ and different values of $V < V_c^{MI}$. For $V \leq 0.5t$ the spectrum is dominated by the Drude peak, in agreement with the optical conductivity observed in the NH_4 salt. The calculations are in qualitative and quantitative agreement with the evolution of the measured optical spectra when going from α-(BEDT-TTF)$_2$NH$_4$Hg(SCN)$_4$ to α-(BEDT-TTF)$_2$KHg(SCN)$_4$, assuming that V/t increases from the former to the latter.[85,127]

4.6.2. β″-(BEDT-TTF)$_2$SF$_5$RSO$_3$

Conductors with the general formula β″-(BEDT-TTF)$_2$SF$_5R$SO$_3$ (R = CH$_2$CF$_2$, CHFCF$_2$, and CHF) show superconducting, insulating, or metallic ground states, depending on the anion. None of them exhibit a Drude peak in the room temperature conductivity, but a wide band with a maximum at about 2000 cm^{-1} is present in the spectra of all the salts and assigned to interband transitions.[130] The compound β″-(BEDT-TTF)$_2$SF$_5$CH$_2$CF$_2$SO$_3$ was studied down to 35 cm^{-1} and a wide electronic band was observed at about 1200 cm^{-1} at $T = 300$ K. Although the fully organic superconductor β″-(BEDT-TTF)$_2$SF$_5$CH$_2$CF$_2$SO$_3$ is metallic from room temperature down to $T_c = 5.2$ K with a well-defined plasma edge at least perpendicular to the stacks, no distinct Drude peak appears in the studied spectral range on cooling as displayed in Figure 26.[39] Decreasing the temperature, the 1200 cm^{-1} electronic band shifts to lower frequencies and its spectral weight grows by several times. Still, $\sigma(\omega)$ drops as $\omega \rightarrow 0$ inferring charge localization. This unusual behavior is attributed to the influence of electronic correlations, and J. Dong et al. suggested[39] that the system is close to a metal-to-insulator transition, despite the superconducting phase transition. This would contradict the tendency found in the α-(BEDT-TTF)$_2M$Hg(SCN)$_4$ salts, as presented in the previous Section 4.6.1.

Raman spectroscopy on β″-(BEDT-TTF)$_2$SF$_5$CH$_2$-CF$_2$SO$_3$ performed at room temperature reveals that the $\nu_3(A_g)$ mode splits into two subpeaks, which were assigned to fractional charges of $+0.41e$ and $+0.59e$, respectively.[131] This result is in excellent agreement with the crystal structure analysis which yields a difference in oxidation state of each donor molecule of ($+0.6e$/$+0.4e$). Similarly for β″-(BEDT-TTF)$_2$SF$_5$-CHFCF$_2$SO$_3$ a slight charge localization of ($+0.47e$/$+0.53e$) was found.

4.6.3. β″-(BEDO-TTF)$_5$[MHg(SCN)$_4$]$_2$

Most two-dimensional compounds of the BEDT-TTF family crystallize in 1:2 stoichiometry and thus are quarter-filled, or half-filled in the case of dimerization. As discussed in Section 4.2, interesting phenomena are expected if the band filling deviates from these simple cases. A one-dimensional Mott−Hubbard insulator will develop a Drude contribution as soon as the filling exceeds 1/2. Within the frame of charge order in two dimensions, a filling different from 1/4 modifies the periodicity. Small deviations from the quarter-filled case prevent the formation of a perfect checkerboard arrangement, for example, making the charge localization less general and dominant.

The study of β″-(BEDO-TTF)$_5$[MHg(SCN)$_4$]$_2$ with M = Cs or Rb provides the possibility to follow changes due to different band filling for the β″-phase salts. Replacing the outer four sulfur atoms in the BEDT-TTF molecules by oxygen—which yields BEDO-TTF—does not change the values U and V considerably. The 1/5-filled compound β″-(BEDO-TTF)$_5$[CsHg-(SCN)$_4$]$_2$ is unique because it shows a nonmetallic temperature dependence of the dc conductivity in one direction of the plane, while in the perpendicular direction the conductivity $\sigma(T)$ remains metallic down to 4 K.[132]

The frequency dependent reflectivity $R(\omega)$ and conductivity $\sigma(\omega)$ in the two polarizations parallel and

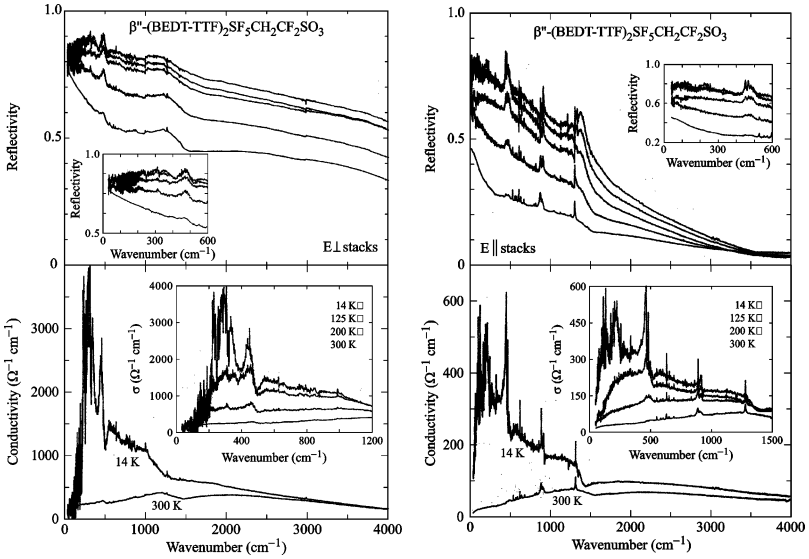

Figure 26. Reflectivity of the organic superconductor β''-(BEDT-TTF)$_2$SF$_5$CH$_2$CF$_2$SO$_3$ for polarizations E perpendicular and parallel to the stacks at different temperatures T = 300, 200, 125, and 14 K (from bottom to top). The corresponding optical conductivity spectra at room temperature and T = 14 K are displayed in the lower frames. The dc conductivity data are indicated by the triangle and square, respectively. The insets magnify the low-frequency behavior. (Reprinted with permission from ref 39. Copyright 1999 American Physical Society.)

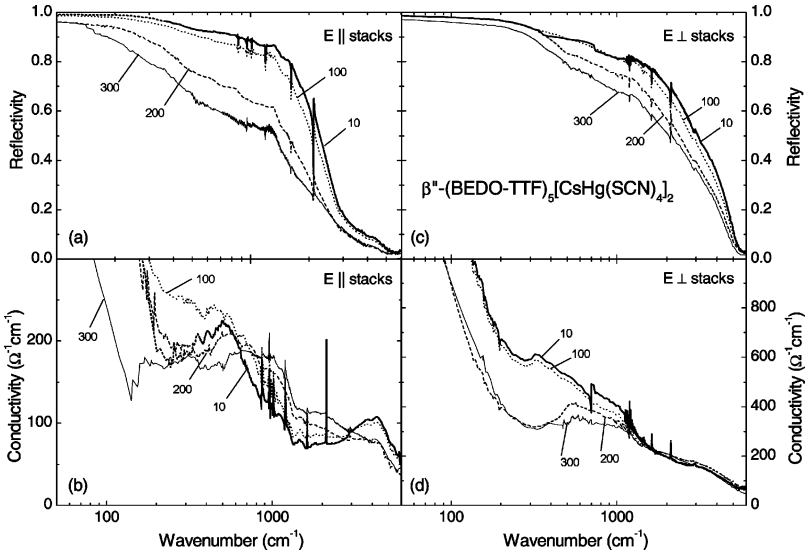

Figure 27. Reflectivity and optical conductivity spectra of β''-(BEDO-TTF)$_5$[CsHg(SCN)$_4$]$_2$ for polarizations E parallel and perpendicular to the stacks at different temperatures T = 300, 200, 100, and 10 K. (From ref 116.)

perpendicular to the stacks of β''-(BEDO-TTF)$_5$[CsHg(SCN)$_4$]$_2$ salts are displayed in Figure 27. In both directions, the 300 K-conductivity spectra consist of a narrow Drude-like component and two broad maxima at 700 and 3000 cm^{-1}. In particular, the presence of the fairly strong zero-frequency feature is in contrast to the quarter-filled structural analogue β''-(BEDT-TTF)$_2$SF$_5$CH$_2$CF$_2$SO$_3$ presented in the previous example (Section 4.6.2). An intensive maximum lies at about 700 cm^{-1}; correspondingly a pseudogap is observed in the spectra at 300 cm^{-1} (Figure 28) The 700 cm^{-1} peak considerably shifts to low frequencies as the temperature decreases (Figure 28) and lies at about 350 cm^{-1} at T = 100 K; thus, the low-frequency gap in $\sigma(\omega)$ becomes less pronounced. The described behavior is basically the same for both polarizations of the electric field, except that for E perpendicular to the stacks the spectral weight of this maximum grows by a factor of 1.5 when going from room temperature to T = 100 K while in the direction parallel to the stacks the intensity of this maximum does not change.

The presence of the low-frequency gap and a maximum in $\sigma(\omega)$ at about 700 cm^{-1} is ascribed to the influence of electron−electron correlations. An essential difference between the previous examples of α-(BEDT-TTF)$_2$[MHg(SCN)$_4$] and β''-(BEDT-TTF)$_2$SF$_5$$RSO_3$ on one hand and β''-(BEDO-TTF)$_5$[CsHg(SCN)$_4$]$_2$ on the other hand is the filling of the conduction band which is 1/4 for the BEDT-TTF compounds and 1/5 for the present system. This deviation from the quarter-filled band leads to the enhancement of the Drude contribution, while the low-frequency gap is still present in the spectra.

The electronic properties of the system can be understood by considering a case in which we dope

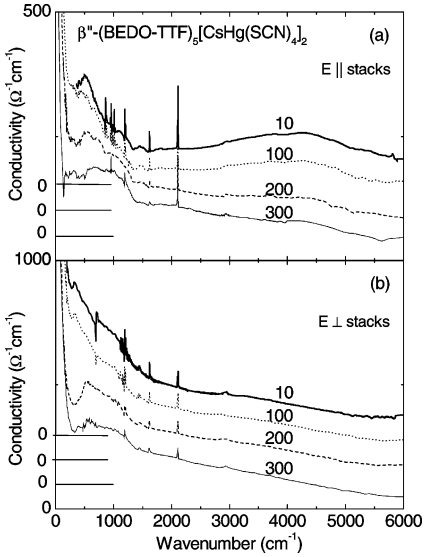

Figure 28. Optical conductivity spectra of β''-(BEDO−TTF)$_5$[CsHg(SCN)$_4$]$_2$ for the polarizations (a) E || *stacks* and (b) $E \perp$ *stacks* for different temperatures as indicated. The curves are shifted for clarity reasons. (From ref 116.)

the insulating checkerboard charge-ordered state with only one hole as discussed by Y. Ohta et al.[133] The single hole (which is an empty site in the checkerboard) has finite probability (for $V > V_c = 2t$ and $U \gg t$), to move to a second-nearest neighbor in the diagonal direction by two successive hopping processes through its nearest neighbors. In a subsequent process, the electron can hop to its third-nearest neighbors and so on. Hence, quasi-particles can disperse with renormalized hopping along the lattice and the system is expected to be always metallic (at a finite value of V). Hence, while at 1/4-filling a metal−insulator transition at a certain V_c^{MI} is expected as discussed in Section 4.6.1, this is not the case at 1/5-filling. Hence, the 1/5-filled salt exhibits a robust Drude component in contrast to the 1/4-filled β''-salts. The short-range checkerboard charge fluctuations, which lead to signatures in the dynamical properties of the 1/4-filled compound — such as the appearance of the low-frequency peak in the optical conductivity, (Figure 25) — as discussed in Section 4.6.1, are also expected to be present in the 1/5-filled system. However, these signatures are somewhat suppressed at 1/5-filling with respect to 1/4-filling for a given value of V because in the former case, the checkerboard charge-ordered state is modified by the presence of mobile empty sites. These arguments are consistent with the observation that, while the spectral weight of the feature appearing at low frequencies in the optical conductivity at 1/4-filling increases by a factor of 5 as the temperature is reduced from room temperature to the lowest temperature, at 1/5-filling this feature is only enhanced by a factor of 1.5.

The behavior of the optical spectra at low frequencies, when going from the 1/4- to the 1/5-filled system, is consistent with exact-diagonalization results. In Figure 29 the behavior of the optical conductivity $\sigma(\omega)$ and the Drude weight at 1/5-filling is plotted for different values of V and for $U = 20t$. The Drude weight remains finite, i.e., the system stays metallic

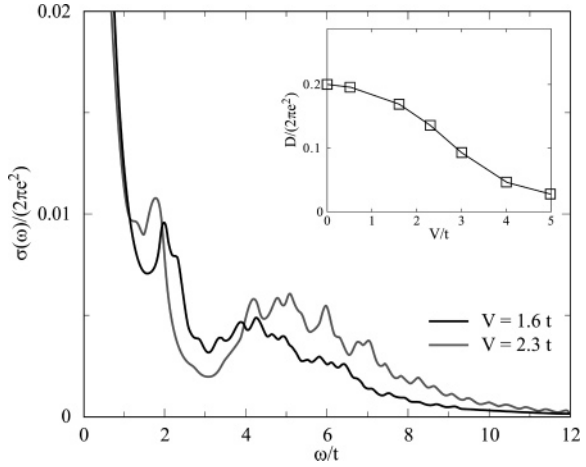

Figure 29. Optical conductivity and Drude weight (inset) from exact diagonalization calculations of an extended Hubbard model on a square lattice. The system is at 1/5-filling, $U = 20t$ and the cluster size is $L = 20$. A broadening of $\eta = 0.2t$ has been used for comparison to experimental data. At 1/5-filling, the system remains metallic for any value of V in contrast with the 1/4-filled salt, which becomes insulating for $V \geq V_c^{MI} \approx 2t$. These calculations are consistent with the strong Drude component observed in the optical conductivity of 1/5-filled salts in contrast to the weaker one found for their 1/4-filled counterparts. Although somewhat suppressed with respect to the 1/4-filled salt, a low-frequency feature is evident for the plotted values of V/t in agreement with experimental observations. (From ref 116.)

for any value of V. This is in contrast to the metal−insulator transition found at $V \approx 2t$ for the 1/4-filled system.[113] The optical conductivity for typical values of V/t exhibits a broad band and a feature at low frequencies, much smaller than the one found for the 1/4-filled case discussed in Section 4.6.1.

5. Superconductivity

Although organic superconductors have been under intensive investigations for two decades, the mechanism of superconductivity and the symmetry of the order parameter are still controversial.[24,134−137] Besides a phonon mechanism, magnetic fluctuations might be important; instead of a simple s-wave symmetry, a d-wave or even triplet p-wave scenarios are discussed. Surprisingly, one of the key experiments for classical superconductors — the optical determination of the superconducting energy gap 2Δ — was successfully performed only recently.[138]

The search for the energy gap by optical means fuelled experimental efforts since the discovery of organic superconductors. Because the two-dimensional BEDT-TTF salts undergo a superconducting phase transition in the range of 10 K,[9] based on the BCS theory[139] the energy gap is expected around $2\Delta/hc = 3.53k_BT_c/hc \approx 25$ cm^{-1}. The relevant temperature and energy range is accessible by high-frequency investigations such as microwaves and far-infrared measurements and by Raman scattering. Here we want to disregard the microwave experiments that have been recently reviewed in ref 140.

Temperature-dependent Raman studies of the phonon dynamics in κ-(BEDT-TTF)$_2$Cu(NCS)$_2$ and κ-(BEDT-TTF)$_2$Cu[N(CN)$_2$]Br corroborate the strong

coupling of the superconducting carriers to intermolecular phonons.[141−143] Due to the interaction of charge carriers with the phonon system, vibrations with $\hbar\omega < 2\Delta$ are expected to soften, while the phonons above the gap frequency become harder below T_c.[144] Accordingly, the low-frequency phonons exhibit an anomalous temperature dependence around and below T_c, which is consistent with an isotropic gap $2\Delta/hc \approx 20$ cm^{-1}.[143] Also inelastic neutron scattering experiments indicate an energy gap in the range of 20−30 cm^{-1},[145,146] supporting the conclusion that intermolecular modes strongly couple to the superconducting charge carriers.

Other spectroscopic methods, such as tunneling,[147] yield an energy gap of $2\Delta/hc \approx 39$ cm^{-1} for κ-(BEDT-TTF)$_2$Cu(NCS)$_2$ at $T = 1.9$ K and the temperature dependence is in full agreement with the BCS prediction. Further results[148−151] vary between samples, but there seems to be structure at around 16 and 32 cm^{-1} that might serve as an indication of an anisotropic energy gap. Other superconducting salts show a similarly inconsistent picture[152,153] as far as the size and the temperature dependence of the gap are concerned. Anisotropic energy gaps (16−80 cm^{-1}) were suggested to interpret the data in ref 151. Recently, T. Arai et al.[154] succeeded to probe the superconducting gap by tunneling spectroscopy in different orientations. For the highly conducting plane the low-energy region could be well fitted by a d-wave symmetry with $2\Delta/k_BT_c \approx 6.7$. In the perpendicular direction, the ratio was between 6.7 and 12.9.

5.1. κ-(BEDT-TTF)$_2$Cu(NCS)$_2$

Measurements of the optical reflection at the superconducting phase transition are extremely difficult since even in the normal state the reflectivity of conducting BEDT-TTF salts in the frequency range below 100 cm^{-1} is much better than 98%, and thus any change at T_c is within the experimental uncertainty of 1%. To overcome these obstacles, J. Eldridge developed a bolometric technique to measure the absorptivity $A = 1 - R$ directly by attaching a Si temperature sensor to the back of the crystal and detect the heating of the sample due to the absorption of light.[32,87,155] If the organic superconductor κ-(BEDT-TTF)$_2$Cu(NCS)$_2$ was cooled below T_c, no change of the optical properties in the frequency range down to 10 cm^{-1} was observed, either by reflection measurements on single crystals,[31,33,88,89] or by transmission experiments on powder samples,[156] or by bolometric techniques.[32,87] In Figure 30 the normalized absorption of κ-(BEDT-TTF)$_2$Cu(NCS)$_2$ is displayed in the frequency range from 10 to 40 cm^{-1}. Within the experimental limit, no significant frequency dependence of the absorption is seen if the temperature decreases below T_c, implying that by optical means no superconducting gap is seen.

Several explanation may be offered: on one hand the transition temperature of these particular crystals may be lower or broadened so much that at 6 K no drop of absorptivity could be observed in this frequency range above 10 cm^{-1}. This would imply $T_c < 7$ K, which is beyond the general experience. On the other hand, κ-(BEDT-TTF)$_2$Cu(NCS)$_2$ may be

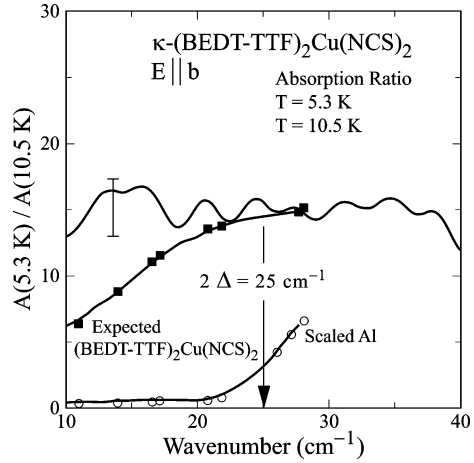

Figure 30. Normalized absorptivity A(5.3 K)/A(10.5 K) of κ-(BEDT-TTF)$_2$Cu(NCS)$_2$ as a function of frequency. The open circles correspond to the absorption of a typical BCS superconductor like aluminum scaled to a transition temperature of $T_c = 10.4$ K. The full squares show the same behavior except with a large residual absorption taken into account as seen by microwave experiments (adapted with permission from ref 32).

in the clean limit, i.e., $2\Delta > \hbar/\tau$, with τ the scattering time. This means that there is no spectral weight in this frequency range which could be changed by the phase transition.[1] Alternatively, the energy gap could be very small compared to the BCS prediction ($2\Delta/hc \approx 25$ cm^{-1}) or even missing, either because the order parameter is anisotropic or the pairing symmetry is not s-wave.

5.2. α_t-(BEDT-TTF)$_2$I$_3$

Only recently, the problem was addressed again by performing optical reflection measurements on α_t-(BEDT-TTF)$_2$I$_3$ because large crystals of more than 5×3 mm^2 are available for this salt which has a transition temperature of $T_c = 8$ K. The crystals are obtained from α-(BEDT-TTF)$_2$I$_3$ by tempering at 70 °C over a period of several hours.[157] The superconducting volume is approximately 15%. Utilizing a coherent source submillimeter spectrometer equipped with backward-wave oscillators operating in the range from 2 to 45 cm^{-1} the reflectivity within the highly conducting plane was studied. The data were complemented by infrared spectra. The low-frequency results at temperatures well above ($T = 15.0$ K) and below ($T = 3.6$ K) the superconducting transition are plotted in Figure 31. In the superconducting state, the reflectivity increases and the conductivity decreases. The transition to the superconducting phase is also unambiguously seen in the frequency-dependent penetration depth of the electromagnetic radiation (inset in Figure 31b).[1] The change in the reflectivity is more obvious in Figure 32a where the ratio is plotted: upon entering the superconducting state a significant increase in reflectivity is observed below 30 cm^{-1} with some undershot up to approximately 60 cm^{-1}.

In Figure 32b, the ratio of the superconducting state and the normal state conductivity is plotted: $\sigma_1^s(\omega, T = 3.6\text{ K})/\sigma_1^n(\omega, T = 15\text{ K})$ taking the effective superconducting volume fraction into account. The

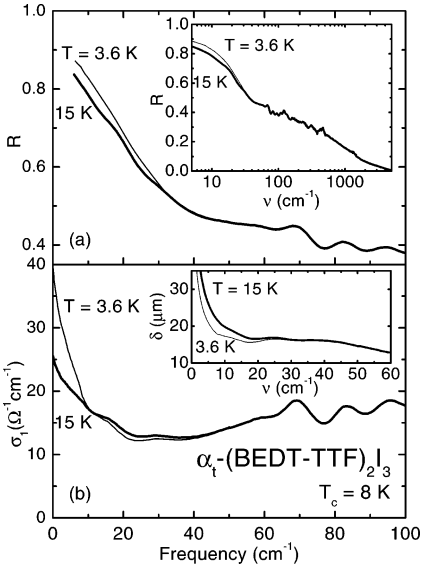

Figure 31. (a) Frequency-dependent reflectivity of α_t-(BEDT-TTF)$_2$I$_3$ at temperatures above and below the superconducting transition ($T_c = 8$ K). The inset shows the reflectivity at $T = 15$ K over a wide spectral range. The inset shows the reflectivity over a wide frequency range. (b) Corresponding conductivity spectra $\sigma(\omega)$ at $T = 15.0$ K and $T = 3.6$ K. The generalized penetration depth δ is plotted in the inset as a function of frequency. (Reprinted with permission from ref 138. Copyright 2002 EDP Sciences.)

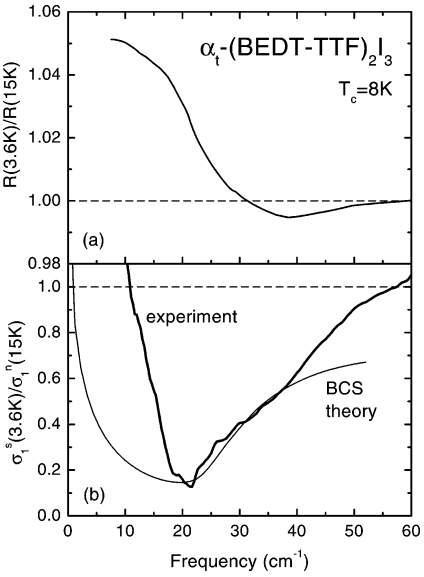

Figure 32. (a) Ratio of the reflectivity spectra of α_t-(BEDT-TTF)$_2$I$_3$ below and above the superconducting transition: $R(\omega, 3.6\text{ K})/R(\omega, 15\text{ K})$. (b) Frequency dependent conductivity $\sigma_1^s(\omega, T = 3.6\ K)$ in the superconducting state normalized to the normal state conductivity $\sigma_1^n(\omega, T = 15$ K). (Reprinted with permission from ref 138. Copyright 2002 EDP Sciences.)

conductivity spectrum clearly shows a dip as predicted by the BCS theory.[1,139] For α_t-(BEDT-TTF)$_2$I$_3$ $2\Delta/hc = (25 \pm 3)$ cm^{-1} or $2\Delta/k_BT_c = 4.4 \pm 0.5$ can be evaluated in good agreement with a medium-to-strong coupling BCS superconductor.

The changes of $\sigma(\omega)$ in the superconducting state are rather weak as compared to conventional superconductors, leading to a correspondingly small spectral weight of the condensate. This spectral weight can be estimated from the missing area in the conductivity spectrum, which we calculate as the difference between the area under the σ_1^n ($T = 15$ K) and the σ_1^s ($T = 3.6$ K) spectra (starting with the frequency 10 cm^{-1}). Thus, the plasma frequency of the condensate is estimated to be $\omega_p^s \geq 25$ cm^{-1}, and also the London penetration depth $\lambda_L = c/\omega_p^s \leq 6\ \mu$m. Magnetization measurements gave $\lambda_L \approx 430$ nm[158] for the in-plane penetration depth. The results are in good agreement with reports of a few micrometers for other BEDT-TTF salts.[24,140]

Resonant Raman experiments on α_t-(BEDT-TTF)$_2$I$_3$ show that the low-energy phonon bands at 32 and 42 cm^{-1} vanish below T_c.[159−161] Since α_t-(BEDT-TTF)$_2$I$_3$ is structurally similar to the β-phase we can apply calculations of the lattice phonons and of the electron−phonon coupling by A. Girlando et al.[41,64] The agreement to the experimental findings is very good, when EMV-coupling with both intra- and intermolecular vibrations is considered.

In conclusion, we can say that the transition to the superconducting state is seen in the optical spectra of organic solids, in the electronic as well as in the vibrational features. The size of the superconducting energy gap and the observed behavior are in agreement with the predictions of the BCS theory. Electron−phonon coupling certainly plays a major role. No indications are found that point in the direction of unconventional pairing mechanism or non-*s*-wave symmetry.

6. Concluding Remarks

During the past 30 years, three major directions of research can be distinguished in the field of molecular conductors: (i) Based on advanced chemistry and materials science new organic compounds were developed and known systems improved to achieve desired properties such as high metallic conductivity, superconductivity at moderate temperatures, or ferromagnetic behavior of appreciable strength. (ii) Various unexpected and unusual phenomena were observed and should be explained, such as density waves, structural changes, charge ordering, superconductivity; the aim is to find the underlying mechanism and theoretical description. (iii) Triggered by theoretical interest, organic compounds serve as model systems to explore physics in reduced dimensions. Due to the possibility of tuning important parameters easily, predictions can be experimentally tested, eventually leading to a deep understanding of low-dimensional physics.

To all of these tasks optical spectroscopy has made important contributions. No doubt, it is one of the most valuable techniques in condensed matter physics in general and in the field of organic conductors in particular. One of the reasons is the large energy range covered, but also the coupling to electronic, vibrational, and even magnetic excitations. Although it has been a standard method for decades, numerous and ongoing improvements make optical measurements even more sensitive and valuable. But also the theoretical analysis and understanding of the data have advanced significantly during the last years.

This review was confined to the influence of electronic correlations on optical properties of two-dimensional organic conductors. Certain BEDT-TTF compounds either undergo a metal-to-insulator transition or show indications of being close to a Mott-insulating phase. This has a severe influence on the electronic and optical properties. Fingerprints of electronic correlations in the room temperature spectra, such as the observation of pseudogaps, may even give indications on the superconducting properties. Under certain circumstances, two-dimensional quarter-filled electron systems are subject to charge ordering. A number of observations can be explained by this phenomenon. For instance, the complete or partial charge localization gives way to an insulating state or the development of a pseudogap in the optical spectrum, or the change of symmetry leads to a splitting of vibrational modes and eventually a shift due to the charge disproportionation. Organic conductors may also serve as model compounds to investigate these phenomena of electronic correlations and charge order because like no other class of solids the parameters of the relative strength of the Coulomb repulsion U/t and V/t can be tuned, and the filling of the conduction band can be varied.

7. Acknowledgments

It is a pleasure to acknowledge fruitful collaboration with M. Dumm, R. Lyubovskaya, J. Merino, J. Schlueter, D. Schweitzer, R. Vlasova, and V. Yartsev. We want to thank the DAAD and the Alexander von Humboldt-Foundation for their generous support.

8. References

(1) Dressel, M.; Grüner, G. *Electrodynamics of Solids*; Cambridge University Press: Cambridge, 2002.
(2) Grüner, G. *Density Waves in Solids*; Addison-Wesley: Reading, MA, 1994.
(3) Sokolov, A. V. *Optical Properties of Metals*; American Elsevier: New York, 1967.
(4) Wooten, F. *Optical Properties of Solids*; Academic Press: San Diego, 1972.
(5) *Metal Optics and Superconductivity*; Golovashkin, A. I., Ed.; Nova Science Publishers: New York, 1989.
(6) Yu, P. Y.; Cardona, M. *Fundamentals of Semiconductors*; Springer-Verlag: Berlin, 1996.
(7) Ferraro, J. R.; Williams, J. M. *Introduction to Synthetic Electrical Conductors*; Academic Press: Orlando, 1987.
(8) Graja, A. *Low-Dimensional Organic Conductors*; World Scientific: Singapore, 1992.
(9) Williams, J. M.; Ferraro, J. R.; Thorn, R. J.; Carlson, K. D.; Geiser, U.; Wang, H. H.; Kini, A. M.; Whangbo, M. H. *Organic Superconductors*; Prentice Hall, Englewood Cliffs, NJ, 1992.
(10) Graja, A. in *Organic Conductors*; J.-P. Farges, Ed.; Marcel Dekker: New York, 1994; p 229.
(11) Jacobsen, C. S.; Tanner, D. B.; Bechgaard, K. *Phys. Rev. B* **1983**, *28*, 7019.
(12) Jacobsen, C. S. *Mat.-Fys. Medd. Dan. Vidensk. Selsk.* **1985**, *41*, 251.
(13) Jacobsen, C. S. *J. Phys. C* **1986**, *19*, 5643.
(14) Jacobsen, C. S. In *Low-Dimensional Conductors and Superconductors*, NATO ASI B Physics Vol. 155; Jérome, D., Caron, L. G., Eds.; Plenum Press: New York, 1987; p 253.
(15) Jacobsen, C. S. In *Low-Dimensional Conductors and Superconductors*, Vol. 27 of *Semiconductors and Semimetals: Highly Conducting Quasi-One-Dimensional Organic Crystals*; Conwell, E., Ed.; Academic: Boston, 1988; p 293.
(16) According to company specifications, the Bruker infrared microscope HYPERION works well down to 80 cm^{-1}.
(17) Kozlov, G.; Volkov, A. In *Millimeter and Submillimeter Wave Spectroscopy of Solids*; Grüner, G., Ed.; Springer-Verlag: Berlin, 1998; p 51.
(18) Eldridge, J. E.; Homes, C. C. *Infrared Phys.* **1989**, *29*, 143.
(19) Homes, C. C.; Reedyk, M.; Cradles, D.A.; Timusk, T. *Appl. Opt.* **1993**, *32*, 2976.
(20) Mair, S.; Gompf, B.; Dressel, M. *Appl. Phys. Lett.* **2004** *84*, 1234. Mair, S. Ph.D. Thesis, Universität Stuttgart, 2003.
(21) Guy, D. R. P.; Marseglia, E. A.; Parkin, S. S. P.; Friedn, R. H.; Bechgaard, K. *Mol. Cryst. Liq. Cryst.* **1982**, *79*, 337.
(22) Jérome, D. In *The Physics and Chemistry of Low-Dimensional Solids*; Alcacer, L., Ed.; Riedel: Dordrecht, 1980; p 123.
(23) Jérome, D.; Schulz, H. J. *Adv. Phys.* **1982**, *31*, 299.
(24) Ishiguro, T.; Yamaji, K.; Saito, G. *Organic Superconductors*, 2nd ed.; Vol. 88 of *Springer Series in Solid-State Sciences*; Springer-Verlag: Berlin, 1998.
(25) Brüesch, P. *Optical Properties of the One-Dimensional Pt Complex Compounds*; In *One-Dimensional Conductors*; Schuster, H. G., Ed.; Lecture Notes in Physics 34; Spinger-Verlag: Berlin, 1975; p 194.
(26) Vescoli, V.; Zwick, F.; Voit, J.; Berger, H.; Zacchigna, M.; Degiorgi, L.; Grioni, M.; Grüner, G. *Phys. Rev. Lett.* **2000**, *84*, 1272.
(27) Tajima, H.; Yakushi, K.; Kuroda, H.; Saito, G. *Solid State Commun.* **1985**, *56*, 159.
(28) Jacobsen, C. S.; Williams, J. M.; Wang, H. H. *Solid State Commun.* **1985**, *54*, 937.
(29) Kuroda, H.; Yakushi, K.; Tajima, H.; Ugawa, A.; Tamura, M.; Okawa, Y.; Kobayashi, A.; Kato, R.; Kobayashi, H. *Synth. Met.* **1988**, *27*, A491.
(30) Tajima, H.; Kyoden, S.; Mori, H.; Tanaka, S. *Phys. Rev. B* **2000**, *62*, 9378.
(31) Kornelsen K.; Eldridge, J. E.; Homes, C. C.; Wang, H. H.; Williams, J. M. *Solid State Commun.* **1989**, *72*, 475.
(32) Kornelsen, K.; Eldridge, J. E.; Wang, H. H.; Williams, J. M. *Phys. Rev. B* **1991**, *44*, 5235.
(33) Eldridge, J. E.; Kornelsen, K.; Wang, H. H.; Williams, J. M.; Crouch, A. V. D.; Watkins, D. M. *Solid State Commun.* **1991**, *79*, 583.
(34) Wang, N. L.; Clayman, B. P.; Mori, H.; Tanaka, S. *J. Phys.: Cond. Matter* **2000**, *12*, 2867.
(35) McKenzie, R. H. *Science* **1997**, *278*, 821.
(36) McKenzie, R. H. *Comments Cond. Mater.* **1998**, *18*, 309.
(37) Merino, J.; McKenzie, R. H. *Phys. Rev. B* **2000**, *61*, 7996.
(38) Merino, J.; McKenzie, R. H. *Phys. Rev. B* **2000**, *62*, 16442.
(39) Dong, J.; Musfeldt, J. L.; Schlueter, J. A.; Williams, J. M.; Nixon, P. G.; Winter, R. W.; Gard, G. L. *Phys. Rev. B* **1999**, *60*, 4342.
(40) Fano, U. *Phys. Rev.* **1961**, *124*, 1866.
(41) Girlando, A.; Masino, M.; Brillante, A.; Della Valle, R. G.; Venuti, E. *Phys. Rev. B* **2002**, *66*, 100507.
(42) Yamaji, K. *Solid State Commun.* **1987**, *61*, 413.
(43) Bozio, R.; Pecile, C. In *Spectroscopy of Advanced Materials*; Wiley & Sons: Chichester, 1991; p 1.
(44) Meneghetti, M.; Bozio, R.; Pecile, C. *J. Phys. I (France)* **1986**, *47*, 1377; *Synth. Met.* **1987**, *19*, 13.
(45) Rice, M. J. *Phys. Rev. Lett.* **1976**, *37*, 36.
(46) Rice, M. J.; Pietronero, L.; Brüesch, P. *Solid State Commun.* **1977**, *21*, 757.
(47) Rice, M. J.; Lipari, N. O.; Strässler, S. *Phys. Rev. Lett.* **1977**, *39*, 1359.
(48) Rice, M. J. *Solid State Commun.* **1979**, *31*, 93.
(49) Rice, M. J.; Yartsev, V. N.; Jacobsen, C. S. *Phys. Rev. B* **1980**, *21*, 3437.
(50) Lipari, N. O.; Duke, C. B.; Bozio, R.; Girlando, A.; Pecile, C.; Padva, A. *Chem. Phys. Lett.* **1976**, *44* 236.
(51) Mori, T.; Kobayashi, A.; Sasaki, Y.; Kobayashi, H.; Saito, G.; Inokushi, H. *Chem. Lett.* **1984**, *1984*, 957.
(52) Yartsev, V. M.; Graja, A. *Int. J. Mod. Phys. B* **1998**, *12*, 1643.
(53) Visentini, G.; Masino, M.; Bellitto, C.; Girlando, A. *Phys. Rev. B* **1998**, *58*, 9460.
(54) Yartsev, V. M. In *Materials and Measurements in Molecular Electronics*; Springer: Berlin, 1996; p 189.
(55) Yartsev, V. M.; Drozdova, O. O.; Semkin, V. N.; Vlasova, R. M.; Lyubovskaya, R. N. *J. Phys. (France) I* **1996**, *6*, 1673.
(56) Yartsev, V. M.; Drozdova, O. O.; Semkin, V. N.; Vlasova, R. M.; Lyubovskaya, R. N. *Phys. Status Solidi B* **1998**, *209*, 471.
(57) Kozlov, M. E.; Pokhodnia, P. I.; Yurchenko, A. A. *Spectrochim. Acta A* **1987**, *43*, 323.
(58) Kozlov, M. E.; Pokhodnia, P. I.; Yurchenko, A. A. *Spectrochim. Acta A* **1989**, *45*, 437.
(59) Eldridge, J. E.; Xie, Y.; Wang, H. H.; Williams, J. M.; Kini, A. M.; Schlueter, J. A. *Mol. Cryst. Liq. Cryst.* **1996**, *284*, 97.
(60) Eldridge, J. E.; Xie, Y.; Wang, H. H.; Williams, J. M.; Kini, A. M.; Schlueter, J. A. *Spectrochim. Acta A* **1996**, *52*, 45.
(61) Eldridge, J. E.; Xie, Y.; Lin, Y.; Homes, C. C.; Wang, H. H.; Williams, J. M.; Kini, A. M.; Schlueter, J. A. *Spectrochim. Acta A* **1997**, *53*, 565.
(62) Eldridge, J. E.; Homes, C. C.; Wang, H. H.; Kini, A. M.; Williams, J. M. *Spectrochim. Acta A* **1995**, *51*, 947.
(63) Eldridge, J. E., private communication.

(64) Girlando, A.; Masino, M.; Brillante, A.; Della Valle, R. G.; Venuti, E. *Horizons in Superconductivity Research*; Nova Science Publisheres: New York, 2004, in press.
(65) Wang H. H.; Ferraro, R.; Williams, J. M.; Geiser, U.; Schlueter, A. *J. Chem. Soc. Chem. Commun.* **1994**, *1994*, 1893.
(66) Wang, H. H.; Kini, A. M.; Williams, J. M. *Mol. Cryst. Liq. Cryst.* **1996**, *284*, 211.
(67) Yamamoto, K.; Yakushi, K.; Miyagawa, K.; Kanoda, K.; Kawamoto, A. *Phys. Rev. B* **2002**, *65*, 085110.
(68) Drozdova, O.; Yamochi, H.; Yakushi, K.; Uruichi, M.; Horiuchi, S.; Saito, G. *J. Am Chem. Soc.* **2000**, *122*, 4435.
(69) Drozdova, O. O.; Semkin, V. N.; Vlasova, R. M.; Kushch, N. D.; Yagubskii, E. B. *Synth. Met.* **1994**, *64*, 17.
(70) Moldenhauer, J.; Horn, C.; Pokhodnia, K. I.; Schweitzer, D.; Heinen, I.; Keller, H. J. *Synth. Met.* **1993**, *60*, 31.
(71) Baker, S. M.; Dong, J.; Li, G.; Zhu, Z.; Musfeldt, J.; Schlueter, J. A.; Kelly, M. E.; Daugherty, R. G.; Williams, J. M. *Phys. Rev. B* **1999**, *60*, 931.
(72) Mori, T. *Bull. Chem. Soc. Jpn.* **1998**, *71*, 2509.
(73) Mori, T. *Bull. Chem. Soc. Jpn.* **1999**, *72*, 179.
(74) Mori, T.; Mori, H.; Tanaka, S. *Bull. Chem. Soc. Jpn.* **1999**, *72*, 2011.
(75) Fortunelli, A.; Painelli, A. *Phys. Rev. B* **1997**, *55*, 16088.
(76) Horiuchi, S.; Yamochi, H.; Satio, G.; Sakaguchi, K.; Kusunoki, M. *J. Am. Chem. Soc.* **1996**, *118*, 8604.
(77) Saito, G. In *Metal−Insulator Transition Revisited*; Edwards, P. P., Rao, C. N. R., Eds.; Taylor & Francis: London, 1995; p 231.
(78) In general, among the BEDO-TTF family there are more metallic salts compared to the BEDT-TTF compounds, indicating a better band overlap by similar values of the Coulomb repulsion.[76]
(79) Kino, H.; Fukuyama, H. *J. Phys. Soc. Jpn.* **1995**, *64*, 4523; Kino, H.; Fukuyama, H. *J. Phys. Soc. Jpn.* **1996**, *65*, 2158.
(80) Seo, H. *J. Phys. Soc. Jpn.* **2000**, *69*, 805.
(81) Yamamoto, T.; Tajima, H.; Yamaura, J.-I.; Aonuma, S.; Kato, R. *J. Phys. Soc. Jpn.* **1999**, *68*, 1384.
(82) Mori, H.; Kamiya, M.; Haemori, M.; Suzuki, H.; Tanaka, S.; Nishio, Y.; Kajita, K.; Moriyama, H. *J. Am. Chem. Soc.* **2002**, *124*, 1251.
(83) Degiorgi, L. *Rev. Mod. Phys.* **1999**, *71*, 687.
(84) Wosnitza, J. *Fermi Surfaces of Low-Dimensional Organic Metals and Superconductors*; Spinger: Berlin, 1996.
(85) Dressel, M.; Drichko, N.; Schlueter J.; Merino J. *Phys. Rev. Lett.* **2003**, *90*, 167002.
(86) Ugawa, A.; Ojima, G.; Yakushi, K.; Kuroda, H. *Phys. Rev. B* **1988**, *38*, 5122.
(87) Kornelsen, K.; Eldridge, J. E.; Wang, H. H.; Williams, J. M. *Solid State Commun.* **1990**, *76*, 1009.
(88) Kornelsen, K.; Eldridge, J. E.; Wang, H. H.; Williams, J. M. *Solid State Commun.* **1990**, *74*, 1501.
(89) Kornelsen, K.; Eldridge, J. E.; Wang, H. H.; Charlier, H. A.; Williams, J. M. *Solid State Commun.* **1992**, *81*, 343.
(90) Vlasova, R. M.; Priev, S. Ya.; Semkin, V. N.; Lyubobskaya, R. N.; Zhilyaeva, E. I.; Yagubskii, E. B.; Yarsev, V. M. *Synth. Met.* **1992**, *48*, 129.
(91) McGuire J. J.; Rõõm, T.; Pronin, A.; Timusk, T.; Schlueter, J. A.; Kelly, M. E.; Kini, A. M. *Phys. Rev. B* **2001**, *64*, 094503.
(92) Petrov, B. V.; Semkin, V. N.; Vlasova, R. M.; Yartsev, V. M.; Kushch, N. D.; Graja, A. In *Molecular Low-Dimensional and Nanostructural Materials for Advanced Applications*; Kluwer, Netherlands, 2002; p 259.
(93) Sasaki, T.; Ito, I.; Yoneyama, N.; Kobayashi, N.; Hanasaki, N.; Tajima, H.; Ito, T.; Iwasa, Y. *Phys. Rev. B* **2004**, *69*, 064508.
(94) Georges, A.; Kotliar, G.; Krauth, W.; Rozenberg, M. J. *Rev. Mod. Phys.* **1996**, *68*, 13.
(95) Haas, P.; Griesshaber, E.; Gorshunov, B.; Schweitzer, D.; Dressel, M.; Klausa, T.; Strunz, W.; Assaad, F. *Phys. Rev. B* **2000**, *62*, R14673.
(96) Griesshaber, E.; Haas, P.; Thoms, J.; Darjushkin, A.; Gorshunov, B. P.; Dressel, M.; Schweitzer, D.; Kremer, R. K.; Golnik, A.; Bernhard, C.; Cardona, M.; Klausa, T.; Strunz, W. *Synth. Met.* **2001**, *120*, 731.
(97) Schiller, M.; Schmidt, W.; Balthes, E.; Schweitzer, D.; Koo, H.-J.; Whangbo, H. H.; Heinen, I.; Klausa, T.; Kircher, P.; Strunz, W. *Europhys. Lett.* **2000**, *51*, 82.
(98) Lieb, E. H.; Wu, F. Y. *Phys. Rev. Lett.* **1968**, *20*, 1445.
(99) Schulz, H. J. In *Strongly Correlated Electronic Materials*; Bedell, K. S., Wang, Z., Meltzer, D. E., Balatsky, A. V., Abrahams, E., Eds.; Addison-Wesley: Reading, 1994; p 187.
(100) Merino, J.; Greco, A.; McKenzie, R. H.; Calandra, M. *Phys. Rev. B* **2003**, *68*, 245121.
(101) Verwey, E. J. W. *Nature* **1939**, *144*, 327. Honig, J. M. In *The Metallic and Non-Metallic States of Matter*; Edwards, P. P., Rao, C. R. N., Eds.; Taylor and Francis: London, 1984; p 261.
(102) Imada, M.; Fujimori, A.; Takura, Y. *Rev. Mod. Phys.* **1998**, *63*, 1.
(103) Goto, T.; Lüthi, B. *Adv. Phys.* **2003**, *52*, 67.
(104) Kuwahara, H.; Tomioka, Y.; Asamitsu, A.; Moritomo, Y.; Tokura, T. *Science* **1995**, *270*, 961; Moritomo, Y.; Asamitsu, A.; Kuwahara, H.; Tokura Y. *Nature* **1996**, *380*, 141.
(105) Rao, C. N. R.; Arulraj, A.; Cheetham, A. K.; Raveau, B. *J. Phys.: Cond. Matter* **2000**, *12*, R83.
(106) Tranquada, J. M.; Sternlieb, B. J.; Axe, J. D.; Nakamura, Y.; Uchida, S. *Nature* **1995**, *375*, 561.
(107) Vojta, M. *Phys. Rev. B* **2002**, *66*, 104505.
(108) Dumm, M.; Basov, D. N.; Komiya, S.; Abe, Y.; Ando, Y. *Phys. Rev. Lett.* **2002**, *88*, 147003.
(109) Nakamura, T.; Minagawa, W.; Kinami, R.; Takahashi, T. *J. Phys. Soc. Jpn.* **2000**, *69*, 504.
(110) Miyagawa, K.; Kawamoto, A.; Kanoda, K. *Phys. Rev. B* **2000**, *62*, R7679.
(111) Takano, Y.; Hiraki, K.; Yamamoto, H. M.; Nakamura, T.; Takahashi, T. *J. Phys. Chem. Solids* **2001**, *63*, 393.
(112) Mori, T. *Bull. Chem. Soc. Jpn.* **2000**, *73*, 2243.
(113) Calandra, M.; Merino, J.; McKenzie, R. H. *Phys. Rev. B* **2002**, *66*, 195102.
(114) McKenzie, R. H.; Merino, J.; Martson, J. B.; Sushkov, O. P. *Phys. Rev. B* **2001**, *64*, 085109.
(115) Wang, N. L.; Mori, H.; Tanaka, S.; Dong, J.; Clayman, B. P. *J. Phys.: Cond. Matter* **2001**, *13*, 5463.
(116) Drichko, N.; Petuhov, K.; Dressel, M.; Bogdanova, O.; Zhilyaeva, E.; Lyubovskaya, R.; Greco, A.; Merino, J. *cond-mat/0309398*.
(117) Mazumdar, S.; Clay, R. T.; Campbell D. K. *Phys. Rev. B* **2000**, *62*, 13400.
(118) Clay, R. T.; Mazumdar, S.; Campbell D. K. *J. Phys. Soc. Jpn.* **2002**, *71*, 1816.
(119) Dressel, M.; Grüner, G.; Pouget, J. P.; Breining, A.; Schweitzer, D. *J. Phys. I France* **1994**, *4*, 579.
(120) Železný, V.; Petzelt, J.; Swietlik, R.; Gorshunov, B. P.; Volkov, A. A.; Kozlov, G. V.; Schweitzer, D.; Keller, H. J. *J. Phys. France* **1990**, *51*, 869.
(121) Wojciechowski, R.; Yamamoto, K.; Yakushi, K.; Inokuchi, M.; Kawamoto A. *Phys. Rev. B* **2003**, *67*, 224105.
(122) Takahashi, T.; Chiba, R.; Takano, Y.; Kubo, Y.; Hiraki, K.; Yamamoto, H.; Nakamura, T. *J. Phys. IV (France) Proc.* **2002**, *12*, Pr9−201.
(123) Mori, H.; Tanaka, S.; Mori, T. *Phys. Rev. B* **1998**, *57*, 12023.
(124) Suzuki, K.; Yamamoto, K.; Uruichi, M.; Yakushi, K. *Synth. Met.* **2003** *135−136*, 525.
(125) Chiba, R.; Yamamoto, H.; Hiraki, K.; Takahashi, T.; Nakamura, T. *J. Phys. Chem. Solids* **2001**, *62*, 389.
(126) Mori, H.; Tanaka, S.; Oshima, M.; Saito, G.; Mori, T.; Maruyama, Y.; Inokuchi, H. *Bull. Chem. Soc. Jpn.* **1990**, *63*, 2183.
(127) Dressel, M.; Drichko, N.; Schlueter, J.; Merino, J. *J. Phys. IV (France) Proc.* **2002**, *12*, Pr9−57.
(128) In α-(BEDT-TTF)$_2$TlHg(SCN)$_4$ indications of a pseudogap are also observed. Drichko, N.; Dressel, M.; Schlueter, J., to be published.
(129) Dressel, M.; Eldridge, J. E.; Wang, H. H.; Geiser, U.; Williams, J. M. *Synth. Met.* **1992**, *52*, 201.
(130) Jobnes, B. R.; Olejniczak, I.; Dong, J.; Pigos, J. M.; Zhu, Z. T.; Garlach, A. D.; Musfeldt J. L. *Chem. Mater.* **2000** *12*, 2490.
(131) Ward, B. H.; Schlueter, J. A.; Geiser, U.; Wang, H. H.; Morales, E.; Parakka, J. P.; Thomas, S. Y.; Williams, J. M.; Nixon, P. G.; Winter, R. W.; Gard, G. L.; Koo, H.-J.; Whangbo, M.-H. *Chem. Mater.* **2000**, *12*, 343.
(132) Drichko, N.; Vlasova, R. M.; Semkin, V. N.; Bogdanova, O. A.; Zhilyaeva, E. I.; Lyuboskaya, R. N.; Lyubovskii, R. B.; Graja, A. *Phys. Status Solidi B* **2003**, *236*, 668.
(133) Ohta, Y.; Tsutsui, K.; Koshibae, W.; Maekawa, S. *Phys. Rev. B* **1994**, *50*, 13594.
(134) Jérome, D. *Science* **1991**, *252*, 1509.
(135) Jérome, D. In *Organic Conductors*; Farges, J.-P., Ed.; Marcel Dekker: New York, 1994; p 405.
(136) Lang, M. *Supercond. Rev.* **1996**, *2*, 1.
(137) Lang, M.; Müller, J. *Organic Superconductors*; In *The Physics of Superconductors*; Bennemann, K. H., Ketterson, J. B., Eds.; Springer-Verlag: Berlin, 2004; Vol. 2, p 453.
(138) Drichko, N.; Haas, P.; Gorshunov, B.; Schweitzer, D.; Dressel, M. *Europhys. Lett.* **2002**, *59*, 774.
(139) Tinkham, M. *Introduction to Superconductivity*, 2nd ed.; McGraw-Hill: New York, 1996.
(140) Dressel, M. In *Studies of High-Temperature Superconductors*; Narlikar, A., Ed.; Nova Science: Huntington, 2000; p 34.
(141) Pedron, D.; Visentini, G.; Bozio, R.; Williams, J. M.; Schlueter, J. A. *Physica C* **1997**, *276*, 1.
(142) Pedron, D.; Bozio, R.; Schlueter, J. A.; Kelly, M. W.; Kini, A. M.; Williams, J. M. *Synth. Met.* **1999**, *103*, 2220.
(143) Faulques, E.; Ivanov, V. G.; Mézière, C.; Batail, P. *Phys. Rev. B* **2000**, *63*, 9291.
(144) Zeyher, R.; Zwicknagl, G. *Solid State Commun.* **1988**, *66*, 617; Zeyher, R.; Zwicknagl, G. *Z. Phys. B* **1990**, *78*, 175.
(145) Toyota, N.; Lang, M.; Ikeda, S.; Kajitani, T.; Shimazu, T.; Sasaki, T.; Shibata, K. *Synth. Met.* **1997**, *86*, 2009.
(146) Pintschovius, L.; Rietschel, H.; Sasaki, T.; Mori, H.; Tanaka, S.; Toyota, N.; Lang, M.; Steglich, F. *Europhys. Lett.* **1997**, *37*, 627.

(147) Bando, H.; Kashiwaya, S.; Tokumoto, T.; Anzai, H.; Kinoshita, N.; Tokumoto, M.; Murata, K.; Kajimura, K. In *The Physics and Chemistry of Organic Superconductors*; Saito, G., Kagoshima, S., Eds.; Springer-Verlag: Berlin, 1990; p 167.
(148) Maruyama, Y.; Inabe, T.; Urayama, H.; Yamochi, H.; Saito, G. *Solid State Commun.* **1988**, *67*, 163.
(149) Maruyama, Y.; Inabe, T.; Urayama, H.; Yamochi, H.; Saito, G. In *The Physics and Chemistry of Organic Superconductors*; Saito, G., Kagoshima, S., Eds.; Springer-Verlag: Berlin, 1990; p 163.
(150) Nomura, K.; Nagao, N.; Ichimuro, K.; Matsunaga, N. *Synth. Met.* **1995**, *70*, 911.
(151) Ichimuro, K.; Arai, T.; Nomura, K.; Takasaki, S.; Yamada, J.; Nakutsuji, S.; Anzai, H. *Synth. Met.* **1996**, *85*, 1543.
(152) Nowack, A.; Poppe, U.; Weger, M.; Schweitzer, D.; Schenk, H. *Z. Phys. B* **1987**, *68*, 41.
(153) Ernst, G.; Nowack, A.; Weger, M.; Schweitzer, D. *Europhys. Lett.* **1994**, *25*, 303.
(154) Arai, T.; Ichimura, K.; Nomura, K.; Takasaki, S.; Yamada, J.; Nakatsui, S.; Anzai, H. *Solid State Commun.* **2000**, *116*, 679; Arai, T.; Ichimura, K.; Nomura, K.; Takasaki, S.; Yamada, J.; Nakatsui, S.; Anzai, H. *Phys. Rev. B* **2001**, *63*, 104518.
(155) Eldridge J. E.; Bates, F. E. *Phys. Rev. B* **1983**, *28*, 6972.
(156) Dressel, M.; Eldridge, J. E.; Williams, J. M.; Wang, H. H. *Physica C* **1992**, *203*, 247.
(157) Schweitzer, D.; Bele, P.; Brunner, H.; Gogu, E.; Haeberlen, U.; Hennig, I.; Klutz, I.; Swietlik, R.; Keller, H. J. *Z. Phys. B* **1987**, *67*, 489.
(158) Gogu, E.; Schweitzer, D.; Keller, H. J. *Physica C* **1988**, *153*−*155*, 491.
(159) Pokhodnia, K. I.; Graja, A.; Weger, M.; Schweitzer, D. *Z. Physik B* **1993**, *90*, 127.
(160) Graja, A.; Pokhodnia, K. I.; Weger, M.; Schweitzer, D. *Synth. Met.* **1993**, *56*, 2477.
(161) Ludwig, T.; Schweitzer, D.; Keller, H. J. *Solid State Commun.* **1995**, *96*, 961.

CR030642F